VITREOUS CARBON TUBE FURNACE FOR ATOMIC FLUORESCENCE SPECTROMETRY

By

CHARLES J. MOLNAR

A DISSERTATION PRESENTED TO THE GRADUATE COUNCIL OF THE UNIVERSITY OF FLORIDA IN PARTIAL FULFILLMENT OF THE REQUIREMENTS FOR THE DEGREE OF DOCTOR OF PHILOSOPHY

UNIVERSITY OF FLORIDA

1974

DEDICATION

This dissertation is dedicated to all my friends, and especially to Jude, the best friend I have ever known.

ACKNOWLEDGMENTS

The author is especially grateful to his research director, Dr. James D. Winefordner, for his advice and encouragement in the course of this research. The scholarly assistance of the members of his committee is also greatly appreciated.

Dr. James D. Winefordner's postdoctoral fellows and graduate students will always be remembered with gratitude for their constructive suggestions and invaluable help.

The author also wishes to acknowledge the technical advice and assistance of Francis D. Ottinger and Arthur P. Grant, as well as the other staff members of the Machine and Instrument Shop.

An expression of thanks is due Gail G. Pokrant for all her help with this and other projects.

TABLE OF CONTENTS

LIST OF TABLES

LIST OF FIGURES

Abstract of Dissertation Presented to the Graduate Council of the University of Florida in Partial Fulfillment of the Requirements for the Degree of Doctor of Philosophy

VITREOUS CARBON TUBE FURNACE FOR ATOMIC FLUORESCENCE SPECTROMETRY

By

Charles J. Molnar

Chairman: James D. Winefordner
Major Department: Chemistry

Resistively heated non-flame cells previously used for atomic absorption and atomic fluorescence spectroscopy are reviewed. A versatile new type of resistively heated non-flame cell usable in both the continuous introduction and the pulsed introduction modes is described, and analytical figures of merit in atomic fluorescence spectrometry are given.

The theory of the conversion of the analyte to an atomic fluorescence signal is reviewed, along with some reasons why non-flame cells in atomic fluorescence spectrometry should attain better signal-to-noise ratios than flame atomic fluorescence spectroscopy. The theories of transient and continuous signals are discussed, and methods to obtain maximum signal-to-noise ratios for each are described.

The design, construction, and evaluation of the new versatile resistively heated non-flame cell are discussed. The non-flame cell system consists of a very efficient pneumatic nebulizer operating at high pressures with low sample consumption for introduction of a fine sample aerosol into a vitreous carbon tube furnace via a desolvation chamber. Atomic vapor of several metals (Sn, Pb, Te, Ag, Tl, and Bi) is produced by continuous pneumatic nebulization of an aqueous sample through a vitreous carbon tube furnace, and atomic fluorescence is excited with single-element electrodeless discharge lamps. The high efficiency of the system is considered along with precision, sensitivity, linear dynamic range, and limits of detection for the elements examined. The decay of atom populations above the furnace outlet using either an Ar-H_2 diffusion flame sheath or an Ar sheath is determined, and the results are discussed.

Pulsed pneumatic nebulization of aqueous samples, containing various metals (Ag, Bi, Cd, Co, Mg, Pb, Sn, Te, Tl, and Zn), into a vitreous carbon tube furnace produced metal vapors which are excited with single-element electrodeless discharge lamps, and the resulting atomic fluorescence is measured. This mode of operation improves the absolute limits of detection; no deleterious effects to the linear dynamic ranges resulted. The concomitant increase in the life of the vitreous carbon tube is also stressed. The

atomic fluorescence intensity versus different sample sizes for a few elements is determined.

Additional advantages of the present non-flame cell system over some past non-flame cells are that operator error due to sample placement is eliminated, and that the conversion of the atomizer from the continuous mode to the pulsed mode of sampling is achieved by simply altering the means of sample injection.

Some areas of future research are discussed. Preliminary results suggest that the present resistively heated non-flame cell offers atomic emission results competitive with some flames. A method for the improvement of the transient signal is discussed. The use of this system for atomic absorption is discussed, along with a possible alteration. Some other areas of future research are discussed.

CHAPTER I

INTRODUCTION

Atomic Absorption Spectroscopy (AAS), Atomic Fluorescence Spectroscopy (AFS), and Atomic Emission Spectroscopy (AES) all depend upon the efficiency of conversion of the sample into the atomic species of interest (the analyte) and the ability to differentiate optically the radiation absorbed or emitted by the analyte (the analytical signal) from all other optical radiation (background). In fluorescence, excitation is a result of absorption of radiation from an external source, whereas in emission excitation is primarily a result of collisional transfer of thermal energy stored in vibrationally excited gaseous molecules, for example, N_2 in flames.

Flames have been in widespread use as atomization cells because they are convenient, reliable (barring flashbacks), and relatively inexpensive. Also, there is a wide variety of flames and commercially available burners which result in high signal-to-noise ratios (S/N) for many elements in the parts per million (ppm) to parts per billion (ppb) concentration range.

The efficiency of flames in converting analyte in the sample solution to gaseous atoms is severely limited for many reasons. To understand the inefficiency (for some elements) of flames as atomizers, one must first have examined the processes which lead to flame atomization, as shown in Figure 1.

With premix burners, the efficiency of transferring the liquid analyte to the flame as a dry aerosol is about 4-5 per cent [1]. The total consumption burner has a larger efficiency of transferring the analyte to the flame as dry aerosol, but has a poorer solute vaporization efficiency [1]. Processes which lead to low atomic concentrations in the flame atomization cell include analyte dilution due to the large flow rates of the fuel and oxidant needed to support flames and gas expansion upon conbustion. Reactions occurring in the flame lead to the formation of many flame gas radicals which may either combine with the analyte to form stable compounds (monoxides of the analyte species resulting from O radicals) or may emit radiation resulting in appreciable background in spectral regions of interest (such as OH, CN, etc.). In some of the higher temperature flames, there occurs significant ionization of some elements, such as Na, K, Cs, Ca, Sr, etc.

Ideally, atomization devices would have high efficiencies of sample transport, low background due to

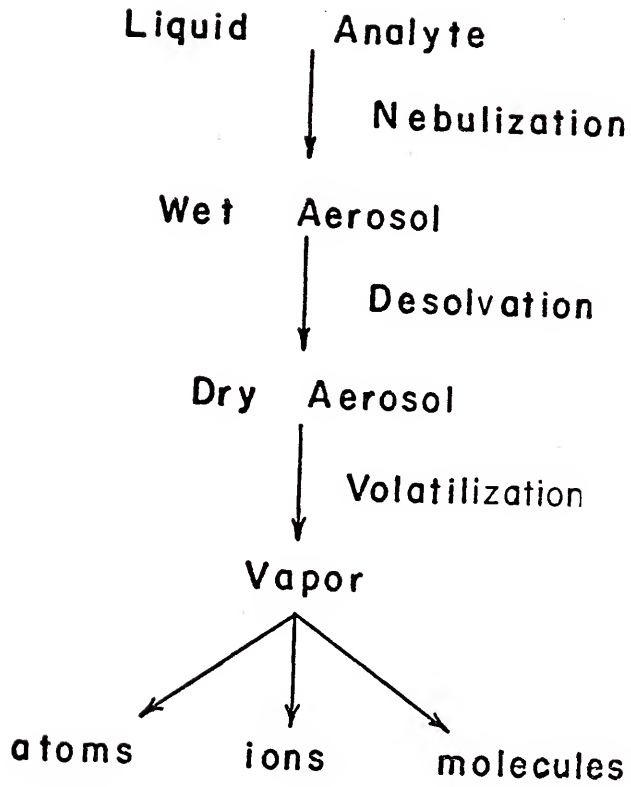

Fig. 1.--Physical process leading to atomic absorption, atomic fluorescence, and atomic emission spectrometry.

emission, and a gaseous environment which would lead to efficient conversion of analyte vapor to analyte atoms. L'vov has been a pioneer in the field of resistively heated non-flame cell spectroscopy; he has used a graphite tube furnace contained in an inert atmosphere for extensive AAS studies [2-6). A complete review of his work is included in his text [7]. Massmann developed a resistively heated graphite cuvette atomization cell suitable for AAS and AFS [8,9]. The AAS system has been developed commercially by Perkin-Elmer; the Perkin-Elmer non-flame cell AAS system has been used to analyze many different elements in complex matrices such as milk [10], sea water [11], oils [12], and blood plasma [13]. Kahn and Slavin [14] increased the sensitivity of this system by stop-flowing the Ar sheath; this system was then further improved by automation of sample introduction by Pickford and Rossi [15], which improved precision from 5-10 per cent to 1-2 per cent.

Samples have also been atomized from carbon filaments into an inert carrier gas by means of resistive heating. West and Williams constructed the first graphite filament atomization device [16] for both AAS and AFS. The filament was first enclosed within a Pyrex cell fitted with quartz windows and purged with Ar. Later, the Pyrex cell was removed and a laminar flow of Ar was used to provide an inert atmosphere about the atomization filament. A number of

elements have been studied with this atomization device [17-27]. Limited field viewing has led to reduced matrix effects [21,22]. Applications have been reported for oil-based solutions [26], Co in soils [28], Mo in organic matrices [27], and V in titanium dioxide [29]. Winefordner et al. described a similar atomization device which was evaluated extensively in AAS and AFS and was used for the analysis of trace metals in both aqueous and oil-based samples [30-34]. The latter non-flame cell was operated in both an Ar and an Ar/H_2 sheath. Studies were carried out on the decay of atomic populations with height above the graphite filament by AAS [32] and AFS [33]. Temperature programming of the filament was used to separate temporally the signals of Ag and Cu in a single cycle [34]; temporal resolution was applied to the analysis of Ag and Cu in jet engine oils.

Amos [35,36] modified the West filament system by drilling a lateral hole through the filament and creating the "Mini Massmann" furnace; he compared the results of AFS to AAS for several elements. Amos found AFS with the graphite filament to result in better limits of detection for many elements than did AAS with the tube non-flame cell; an Ar/H_2 diffusion flame was used to shield the atomized elements. The "Mini Massmann" furnace has become the commercial Varian non-flame atomization device on which

application studies for elements in oils [37], Se in natural waters [38], and Ag and Au in metallurgical samples [39] have been reported. Bratzel and Chakrabarti [37] measured the temperature of the atomic vapor produced in the Varian type of non-flame cell and found that thermal equilibrium did not exist, which is not surprising in a system containing so few molecules to aid the attainment of equilibrium.

Brandenburger and Bader were the pioneers in using resistively heated metal filaments as atomization devices [40]. Bratzel, Dagnall, and Winefordner employed a resistively heated Pt filament for use as an atomization source for AFS with excellent results for some volatile elements [41]. Hwang et al. [42] used a resistively heated tantalum strip in an enclosed inert atmosphere to analyze Pb in blood serum. They also reported the determination of thirty-seven elements by AAS [43].

Few resistively heated non-flame cells with continuous-sample introduction have been reported. Woodriff et al. [44 - 46] employed either continuous pneumatic nebulization of the cold aerosol into a resistively heated graphite tube furnace or discrete sampling via sample placement with a microliter syringe into a resistively heated graphite tube. Applications using the discrete sampling mode were performed on Ag in snow [47], Pb in air [48], and Pb in fish [49]. M. S. Black et al. [50] evaluated two types of platinum tube

furnaces with continuous pneumatic nebulization for AFS; no applications of this system to real samples were described. M. K. Murphy, S. A. Clyburn, and C. Veillon developed a unique pyrolytic carbon tube furnace for use in AFS [51]; this system resulted in sub-parts per billion (ppb) limits of detection for some elements. The latter two non-flame cells utilized a Veillon-Margoshes sample aerosol injection system [52].

Non-flame cells other than the resistively heated non-flame cell types have been employed in various types of atomic spectroscopy, but they will not be discussed here. The interested reader may consult the excellent reviews of non-flame cells by Winefordner [53], Kirkbright [54], and Winefordner and Vickers [55] for a thorough discussion of these, as well as the previously mentioned resistively heated non-flame cell studies.

The purpose of this research project was to develop an efficient, versatile non-flame atomization cell for use in atomic fluorescence spectroscopy. This entailed the development of a new high pressure, low sample consumption pneumatic nebulizer which was coupled to a vitreous carbon tube non-flame cell via a desolvation chamber into which the analyte was introduced either in the continuous or pulsed modes. The resulting system was evaluated as an atomizer for atomic fluorescence spectrometry. Analytical

figures of merit are given for several elements, and the possible use of the atomizer for emission spectroscopy is also discussed.

CHAPTER II

THEORETICAL CONSIDERATIONS

Types of Atomic Fluorescence Transitions

Resonance fluorescence transitions involve identical lower and upper levels in the excitation-de-excitation processes. Direct line fluorescence involves only the same upper level in the radiational excitation-de-excitation processes. Stepwise line fluorescence involves different upper levels in the radiational excitation-de-excitation processes. If the fluorescence energy exceeds the excitation energy, the fluorescence is termed an Anti-Stokes process, and if the reverse is true, the fluorescence transition is then called a Stokes process. A few types of atomic fluorescence have been shown in Figure 2. For a more extensive discussion of the types of fluorescence, and where they have been observed, one should consult the article by Omenetto and Winefordner [56].

Intensity of Atomic Fluorescence

The intensity of atomic fluorescence emitted from the analyte depends principally upon: the intensity of the exciting radiation; the concentration of the analyte in the

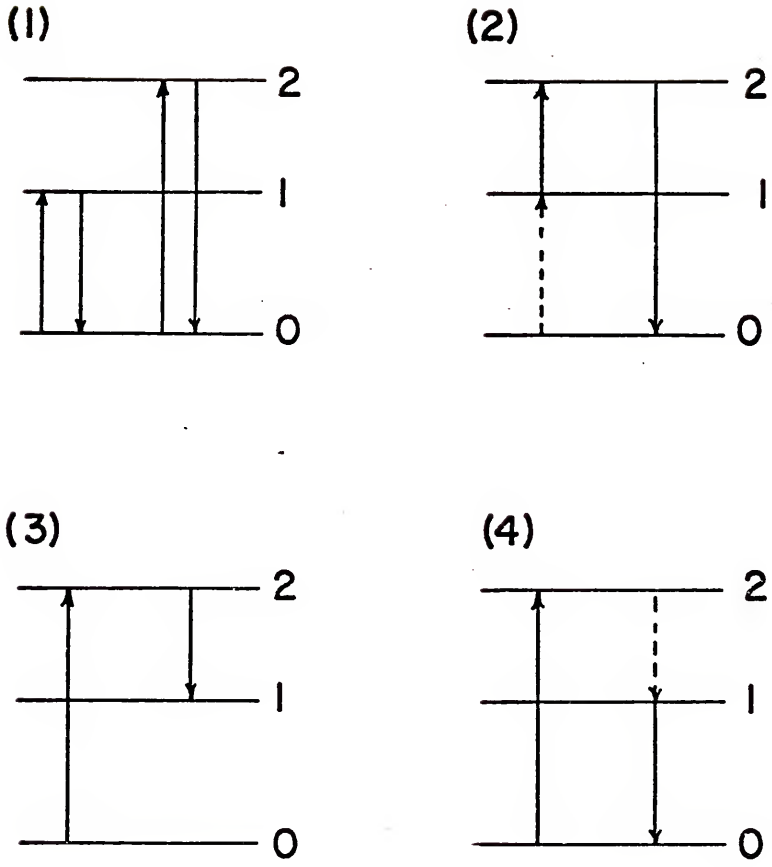

Fig. 2.--Types of atomic fluorescence.

(1) Resonance fluorescence.
(2) Anti-Stokes direct line fluorescence.
(3) Stokes direct line fluorescence.
(4) Stokes stepwise line fluorescence.

atom cell; the efficiency of the conversion of absorbed radiation into the emitted radiation (quantum efficiency); and the ratio of the excitation source half-width to the absorption line half-width. If it is assumed that the source excitation is imaged on the atomic vapor exiting from the atomizer (atom cell), that the atom cell completely collects all source excitation, and that the solid angle of the monochromator is filled by the fluorescence of the atom cell, then the most general equation for the integrated fluorescence radiance (intensity) B_F, for an isolated spectral line is

$$B_F = \frac{E_A Y'}{4\pi} \left(\frac{Ll'}{A_S}\right) \qquad \text{II-1}$$

where B_F is the fluorescence radiance (erg $sec^{-1}cm^{-2}sr^{-1}$), L is the fluorescence path length (cm), l' is the atom cell height (cm), A_S is the total atom cell surface area (cm^2), E_A is the total irradiance per unit area absorbed by the spectral line which results in fluorescence (erg $sec^{-1}cm^{-2}$), and Y' is the quantum efficiency (watts emitted by fluorescence to the watts of the source power absorbed per unit area).

The irradiance absorbed by the analyte in an atom cell is given by

$$E_A = \Omega_A \sum_i B_{S_i} K_{T_i} \qquad \text{II-2}$$

where Ω_A is the solid angle over which the excitation occurs, Σ_i is the summation over all i of $(B_i\ K_i)$, B_S is the incident spectral radiance of the exciting radiation (erg $sec^{-1}cm^{-2}sr^{-1}$), and K_{T_i} is the total absorption factor (sec^{-1}) for different absorbing lines i. If, as in this study, only resonance fluorescence is of interest, then Equation II-2 may be simplified to

$$E_A = \Omega_A\ B_S\ K_T \qquad \text{II-3}$$

where B_S and K_T are values evaluated at the resonance frequency.

Winefordner et al. [57-59] have rigorously derived the expressions for the intensity of atomic fluorescence when using either a line or continuum source at low and high optical densities in the atom cell. Figure 3 shows schematically the atom cell, the source intensity direction, and the direction in which fluorescence is measured. Assuming the following conditions for fluorescence from an atom cell:

1. The sample cell is completely illuminated,
2. The fluorescence radiation is collimated and at right angles to the source radiation,
3. The atomic concentration is homogeneous throughout the sample cell,
4. The temperature is homogeneous throughout the sample cell,
5. Only resonance fluorescence contributes to the fluorescence radiance,

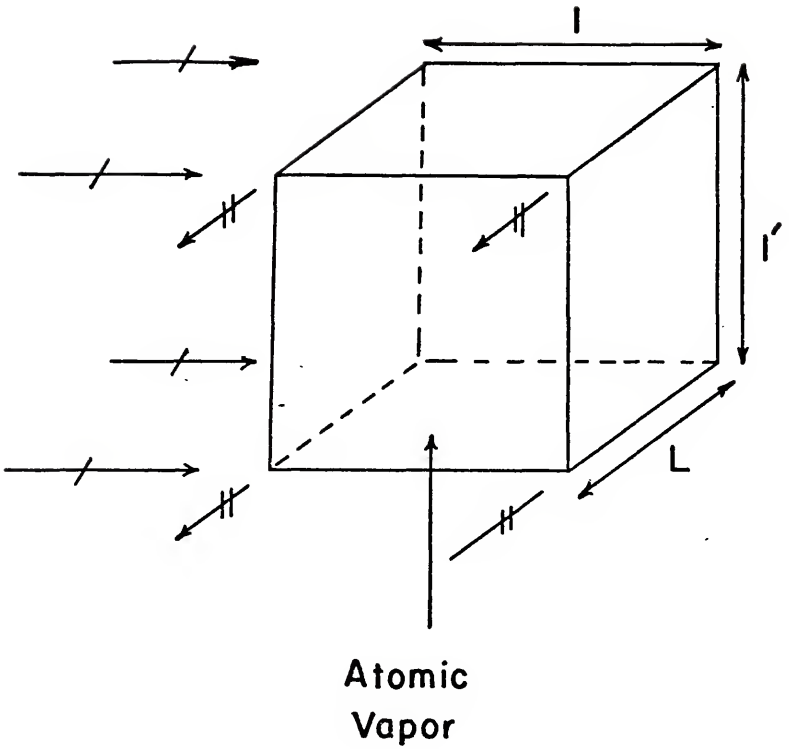

Fig. 3.--Schematic diagram of the atom cell.

—/→ = source radiation.

—//→ = fluorescence radiation.

l,l',L = for definitions, see text.

the intensity of fluorescence may be calculated. If a line excitation source is used, the following equation holds for the atomic fluorescence radiance, B_F (erg $sec^{-1}cm^{-2}sr^{-1}$) at low analyte concentrations (n_o) [57,58] where the total absorption factor, K_T, has been evaluated

$$B_F = K_{lu}\, n_o X_l f_{lu}\, \delta_{lu}\, B_S Y' \left(\frac{\Omega}{4\pi}\right)\left(\frac{L l l'}{A_S}\right) \qquad \text{II-4}$$

where

K_{lu} = modified atomic absorption coefficient for pure Doppler broadening (cm^2)

n_o = concentration of the atoms in the ground state (cm^{-3})

X_l = fraction of analyte atoms in the lower state involved in the absorption transition (dimensionless)

f_{lu} = absorption oscillator strength for transition $l \longrightarrow u$, where l is the lower state and u is the upper state (dimensionless)

δ_{lu} = factor to account for finite half-width of the line source compared to the absorption line (dimensionless)

Ω = solid angle of source radiation collected and impinging upon the flame (sr)

l = absorption path length (cm).

For high optical densities, the following equation is derived for excitation with a line source [57,58]

$$B_F = 2\, B_S\, l'\, Y' \left(\frac{\Omega}{4\pi}\right) \sqrt{\frac{a_F L}{\pi\, K_F\, n_o X_F f_F}} \left(\frac{1}{A_S}\right) \qquad \text{II-5}$$

where

a_F = damping constant for atomic fluorescence (dimensionless)

K_F = modified absorption coefficient (same as K_{lu}), but for reabsorption of fluorescence (cm^2)

X_F = fraction of atoms in the lower state involved in the reabsorption of fluorescence (dimensionless)

f_F = absorption oscillator strength for reabsorption of fluorescence (dimensionless).

If a continuum source of radiation is used to excite resonance fluorescence, then the atomic fluorescence radiance, B_F, for low analyte concentrations, n_o, is equal to [57,58]

$$B_F = C_1\, K_{lu}\, n_o\, X_1\, f_{lu}\, \Delta\lambda_D\, B_{C\lambda_{lu}}\, Y' \left(\frac{\Omega}{4\pi}\right)\left(\frac{L l l'}{A_S}\right) V \qquad \text{II-6}$$

where

$C_1 = \pi\ (2 \ln \sqrt{2})$ (dimensionless)

$\Delta\lambda_D$ = Doppler half-width of the absorption line (nm)

λ_{lu} = absorption line peak for transition $l \longrightarrow u$ (cm)

$B_{c\lambda_{lu}}$ = spectral radiance for a continuum source (erg $sec^{-1}cm^{-2}sr^{-1}nm^{-1}$).

At high analyte concentrations, n_o, the atomic fluorescence radiance, B_F, is equal to [57,58]

$$B_F = 2\, B_{c\lambda_{lu}} \Delta\lambda_D\, a_F\, l'\, Y' \left(\frac{\Omega}{4\pi}\right)\left(\frac{C_2 L l}{\sqrt{\pi}}\right)^{1/2} \left(\frac{1}{A_S}\right) \qquad \text{II-7}$$

where

$C_2 = \sqrt{\pi}\ (\ln 2)^{-1}$ (dimensionless).

The experimental analytical growth curves for atomic fluorescence with a line excitation source and a continuum excitation source have been measured and the low and high concentration asymptotic regions have been compared with the above equations by Winefordner et al. [60,61]. Theoretical growth curves are shown in Figures 4 and 5. It should be noted from these growth curves that atomic fluorescence spectroscopy is most useful analytically for low concentrations of analyte, n_o, in the atom cell because the sensitivity (slope of the analytical curve) is greatest in that region, approaching an asymptote of 1 for both continuum and line source excitation of atomic fluorescence. For high analyte concentrations, the fluorescence radiance is independent of analyte concentration for continuum source excitation and depends upon $\frac{1}{\sqrt{n_o}}$ for a line source excitation.

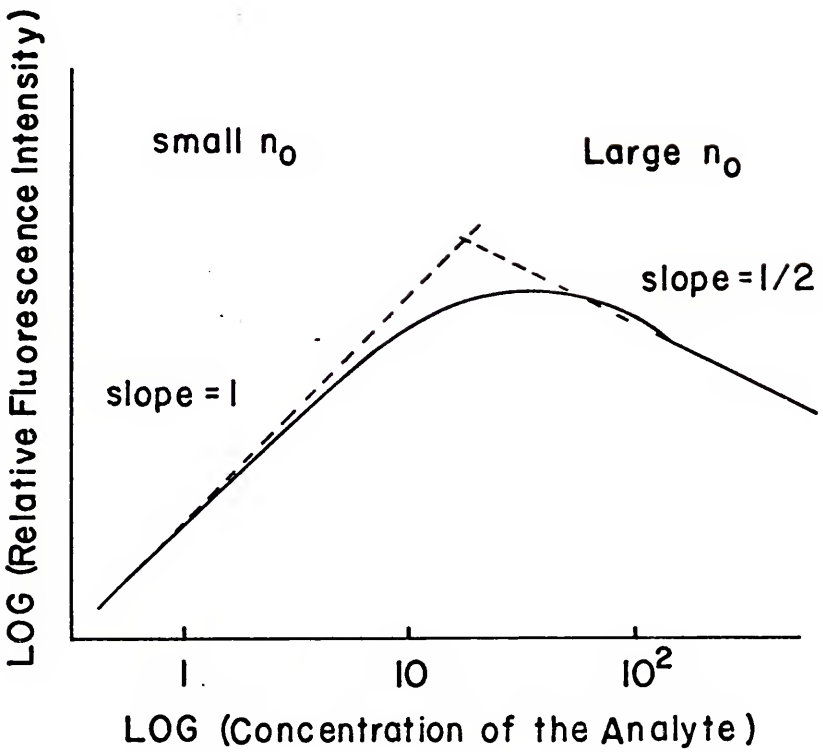

Fig. 4.--Atomic fluorescence growth curve with a line source of excitation.

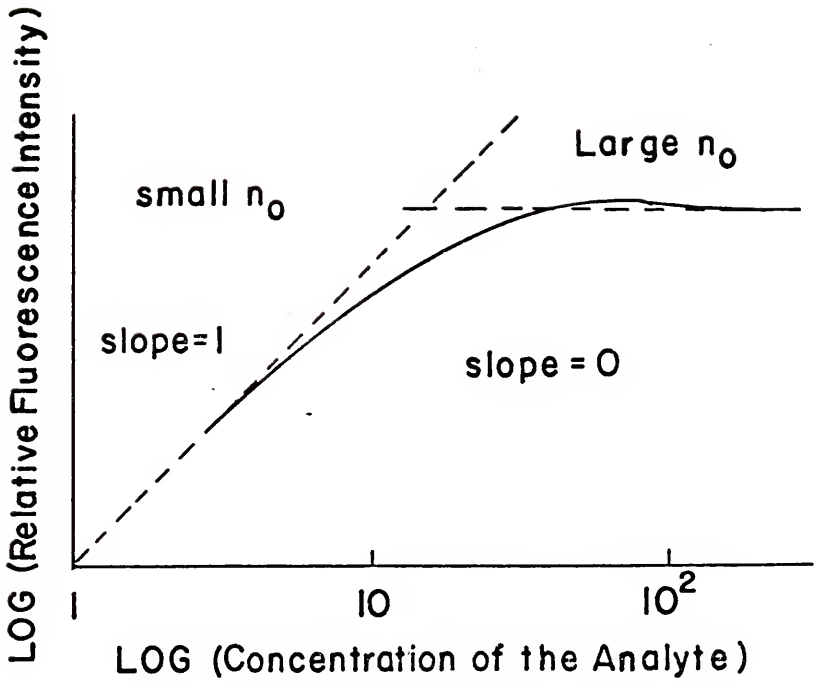

Fig. 5.--Atomic fluorescence growth curve with a continuum source of excitation.

Fluorescence Quenching Considerations

The species in a resistively heated non-flame cell should have a much lower quenching efficiency for the excited-state atoms than does a combustion flame, mainly due to the difference in the gaseous environments (that is, an inert atomic gas in the non-flame cell (Ar, He, etc.) versus molecular species in the flame (N_2, CO, CO_2, etc.) [53]. This should lead to more intense fluorescence from a resistively heated non-flame cell than from a flame (assuming equal atom concentrations and source characteristics to be the case) by a factor of

$$Q = \frac{Y'_{n\cdot F}}{Y'_F} \qquad \text{II-8}$$

where the $Y'_{n\cdot F}$ is the quantum efficiency of fluorescence of the analyte in the non-flame cell and Y'_F is the quantum efficiency of fluorescence of the analyte in the flame. This ratio has been expressed [53] as

$$Q = \frac{[K_F + \Sigma_i (K_{Q_i} n_{Q_i})_{n-F}]}{[K_F = \Sigma_i (K_{Q_i} n_{Q_i})_F]} \qquad \text{II-9}$$

where k_F is the first-order rate constant for radiational deactivation of the resonance level (sec^{-1}), k_{Q_i} is the second-order quenching rate constant for deactivation of the resonance level by collisions of element Z with a quencher Q_i ($cm^{-3}sec^{-1}$), and h_{Q_i} is the concentration of the

quencher (cm^{-3}). The concentration of the quenching species is at a minimum in the inert atmospheres of non-flame cells, and thus

$$k_F >> \Sigma_i \, (k_{Q_i} \, n_{Q_i})_{n-F} \qquad \text{II-10}$$

This leads to [53]

$$Q = \frac{k_F}{k_F + \Sigma_i \, (k_{Q_i} \, n_{Q_i})_F} \qquad \text{II-11}$$

For many common analytical flames [62-64], and for a typical inert atmosphere non-flame cell, the ratio Q is given by

$$Q = \frac{k_f}{\Sigma_i \, k_{Q_i} \, n_{Q_i}} \qquad \text{II-12}$$

which leads to the conclusion that the analyte should emit fluorescence approximately ten times more intensely in the inert atmosphere of a non-flame cell, compared to a flame cell (keeping in mind the assumption of the same atom concentrations in both cells and equivalent sources of excitation).

Noise Considerations

The major sources of noise in atomic fluorescence flame spectroscopy are flame flicker noise and phototube photonoise. With higher temperature, fuel-rich flames, flame flicker noise may be several orders of magnitude

larger than shot noise, hence increasing the lowest concentrations which may be observed by atomic fluorescence flame spectroscopy. The total noise, Δi_{tot}, for various individual sources of random noise Δi_1, Δi_2...., is

$$\Delta i_{tot} = \sqrt{\Delta i_1^2 + \Delta i_2^2 + \ldots} \qquad \text{II-13}$$

When using a properly baffled resistively heated non-flame cell which prevents the black-body radiation of the hot carbon from reaching the photomultiplier, the atomic fluorescence measurement is limited by shot noise, thus providing another advantage of resistively heated non-flames as atomization devices over flames.

Atom Generation and Signal Measurement

Once the physical processes which constitute atomic fluorescence and the parameters which govern the intensity of fluorescence have been understood, one must decide how atomic population is to be produced and how the analytical signal should be measured. This was covered in great depth for transient atom populations by L'vov [65]. If N_o is the number of atoms of the analyte consumed, N is the total number of atoms of the analyte in the atom cell at time, t, τ_1 is the duration of transfer of atoms into the cell, τ_2 is the average residency time of analyte in the cell, and τ_3 is the time the signal is recorded for, then

$$\frac{dN}{dt} = n_1(t) - n_2(t) \qquad \text{II-14}$$

where $n_1(t)$ is the number of atoms entering the cell at time, t, and $n_2(t)$ is the number of atoms escaping from the cell at time, t. For transient sample introduction

$$n_1(t) = N_o/\tau_1 \qquad \text{II-15}$$

and

$$n_2(t) = (\frac{W}{V})\ N \qquad \text{II-16}$$

$$n_2(t) = \frac{N}{\tau_2} \qquad \text{II-17}$$

where W/V was the ratio of the flow rate of the aspiration gas (1 sec^{-1}) to the volume of the atomization cell (1).

Thus, the equation relating the change of atomic populations to change in time is

$$\frac{dN}{dt} = \frac{N_o}{\tau_1} - \frac{N}{\tau_2} \qquad \text{II-18}$$

It is recognized that for $\tau_1 >> \tau_2$, the magnitude of N(t) approaches a constant value or that [65]

$$\frac{dN}{dt} = 0 \qquad \text{II-19}$$

From Equation II-19, it followed from Equation II-18 that

$$N_{eq} = (\frac{\tau_2}{\tau_1})N_o \qquad \text{II-20}$$

It has been widely recognized that electronic circuits may distort the original pulse shape. From the theory of electronic circuits [65,66], the relationship

between the distorted peak shape i(t) to the original peak shape, N(t), and the transient characteristics of the network A(t) is given by

$$i(t) = N(0) \times A(t) + \int_0^t A(t-\tau)N'(\tau)\delta\tau \qquad \text{II-21}$$

where N'(t) is an integration variable, N'(t) is a derivative function of N(t) where t has been replaced by the variable, τ, and N(0) is the value of the function N(t) at time t=0. The time constant, τ_c, is defined for a simple RC circuit by

$$\tau_c = RC \qquad \text{II-22}$$

where τ_c is the length of time during which the output signal is within 36.8 (that is, 100 x e^{-1}) per cent of the input signal and R is the resistance (ohms), and C is the capacitance (Farads). The transient characteristic of the circuit passing from unity voltage-to-0 is

$$A(\tau) = \exp\left(-\frac{\tau}{\tau_c}\right) \qquad \text{II-23}$$

and the 0-to-unity voltage transient is

$$A_t = 1 - \exp\left(-\frac{t}{\tau_c}\right) \qquad \text{II-23a}$$

To obtain the highest value of signal-to-noise, L'vov [65] experimentally showed that the time constant of the measurement circuit, τ_c, should be approximately equal to the value of τ_2, the average residency time of the

analyte in the cell for a transient signal. He also stressed that the analyst may increase precision of his analytical measurements by using integration techniques for signal measurement rather than just peak heights.

For continuous-sample introduction, the magnitude of N(t) approaches a constant value, or

$$\frac{d\,N(t)}{d\,t} = 0 \qquad \text{II-24}$$

Thus, when measuring the equilibrium signal from a continuous-sampling atomization cell, the time constant, τ_c, of the recording device may be adjusted to a larger value than when measuring a transient signal; the larger τ_c reduces the measured noise through time averaging and also increases the analysis time, and hence the amount of analyte consumed. At least five time constants should elapse before performing any analytical signal measurements, to allow the signal to reach greater than 95 per cent of its maximum value.

Concentration of Analyte in the Atom Cell

For the pulsed mode of sample introduction, it will be assumed that the analyte is exponentially diluted. Therefore, the concentration of analyte atoms in the atom cell, n_t, at any time, t, is [67]

$$n_t = n_o\, e^{-(u\,t/V)} \qquad \text{II-25}$$

where

t = time (sec)

V = volume of the exponential dilution flask (cm^3)

u = flow rate of aspirating gas ($cm^3\ sec^{-1}$)

n_t = concentration of analyte at time, t, in the atom cell (cm^{-3})

n_o = initial concentration at time t = 0 of analyte in the atom cell (cm^{-3})

The initial concentration, n_o, in the atom cell can be estimated if it is assumed that the entire pulse of analyte atoms enters the exponential dilution flask and reaches a homogeneous concentration before any analyte exits and so [53]

$$n_o = \frac{v\ c\ N_A \epsilon \beta\ Z_T}{V e_F} \qquad \text{II-26}$$

where

v = volume of sample solution pulse (cm^3)

V = volume of exponential dilution flask (cm^3)

c = concentration of analyte in sample solution prior to aspiration (mol cm^{-3})

N_A = Avogadro's number (mol^{-1})

ϵ = efficiency of aspiration (dimensionless)

β = free atom fraction (dimensionless)

e_F = gas expansion factor (dimensionless)

Z_T = ratio of atoms in ground state to total number in all states (dimensionless)

For the continuous-sampling flame (or non-flame cell) system, the concentration, n, of the analyte atoms in the atom cell (atoms cm^{-3}) is related to the concentration, c, of the analyte (mol l^{-1}) aspirated into the flame by [53]

$$n = 1 \times 10^{19} \left(\frac{F \epsilon \beta c}{Qe_F}\right) Z_T \qquad \text{II-27}$$

where

F = sample flow rate (cm^3 min^{-1})

ϵ = same as defined above

β = same as defined above

e_F = same as defined above

Q = flow rate of the gas entering atom cell (cm^3 sec^{-1})

Z_T = the ratio of atoms in the ground state to the total number of atoms in the atom cell (dimensionless).

The aspiration efficiency, ϵ, is the ratio of the number of atoms of analyte entering the nebulizer to the total number of gaseous analyte atoms contained in the atom cell. This factor corrects for losses of analyte solution in the nebulizer and associated tubing, and the incomplete volatilization of the solid particles in the atom cell.

The free atom fraction, β, is the ratio of the number of analyte atoms in any form to analyte atoms in all gaseous forms in the atom cell. This factor corrects for incomplete

dissociation of the analyte compound, combination of analyte atoms with flame gas radicals, condensation of the analyte atoms to form the original compounds, and ionization of the analyte atoms.

The factor Z_T accounts for the proportion of free atoms contained in the atom cell which are not in their electronic ground state and may be evaluated with the Boltzmann equation [68]

$$\frac{n_s}{n_o} = \frac{g_s}{g_o} e^{-E_s/kT} \qquad \text{II-28}$$

where

n_o = number of atoms in the ground state (dimensionless)

n_s = number of the atoms in a level with an excitation energy of E_s (dimensionless)

g_s, g_o = weighting factors (dimensionless)

k = Boltzmann's constant (8.614×10^{-5} eV $°K^{-1}$)

T = atom cell temperature (°K)

E_s = excitation energy of levels (eV)

The total atom concentration will be, n_T,

$$n_T = n_o + n_1 + n_2 + \cdots \qquad \text{II-29}$$

and so from Equation II-29 and the Boltzmann equation (Equation II-28)

$$n_T = \frac{n_o}{g_o}\left[g_o + g_1 e^{-E/kT} + g_2 e^{-E_2/kT} + \ldots\right] \qquad \text{II-30}$$

$$= \frac{n_o}{g_o}(B) \qquad \text{II-31}$$

where

$$B = g_o + g_1 e^{-E_1/kT} + g_2 e^{-E_2/kT} + \ldots \qquad \text{II-32}$$

and finally Z_T is

$$Z_T = \frac{g_o}{B} \qquad \text{II-33}$$

Limit of Detection Considerations

A very useful analytical figure of merit for use in trace element analysis is the limit of detection (LOD), which is defined statistically so that comparisons may be carried out between different methods of analysis. The statistical theory used here was developed by Kaiser [69-71]. The limit of detection, $\underline{C}$, is defined as

$$\underline{C} = m\underline{S} \qquad \text{II-34}$$

where m is the slope of the analytical curve $m = \frac{d(\log C)}{d(\log S)}$ (S is the signal resulting from a concentration of analyte, C) and is assumed to be constant from the LOD to 1000 x LOD. The smallest analyte signal measurable ($\underline{S}$) is

$$\underline{S} = \bar{S}_{s+b} - \bar{S}_b \qquad \text{II-35}$$

where $\bar{S}_{s+b}$ is the average limiting signal due to the analyte plus blank and $\bar{S}_b$ is the average blank signal. Generally,

$\underline{S}$ is further defined in terms of the fluctuations of the signal. The standard deviation of these fluctuations is defined by

$$\sigma_{\underline{S}} = \sqrt{\frac{\sigma_b^2}{n_b} + \frac{\sigma_{s+b}^2}{n_s}} \qquad \text{II-36}$$

where σ_b is the standard deviation of the blank signal, σ_{s+b} is the standard deviation of the signal plus blank signal, n_b is the number of measurements performed on the blank signal, and n_s is the number of measurements performed on the analyte signal (plus blank). At the limit of detection, the σ_b will approximate σ_{s+b}. The limiting detectable signal is then

$$\underline{S} = Z\,\sigma_{\underline{lim}} \qquad \text{II-37}$$

where Z is the z-statistics of the normal distribution, that is, a protection factor. If the number of observations are large (about 20), then Z may be replaced by the Student t and $\sigma_{\underline{S}}$ by s_s which is the estimated standard deviation of the signal near the limit of detection. If $n_s = 1$ and $n_b \geq 15$, then Equation II-36 may be reduced to

$$\underline{C} = m \cdot ts_b \qquad \text{II-38}$$

where s_b is the estimated standard deviation of the blank and if $s_b \approx s_s$. However, if $n_s \approx n_b$, then Equation II-36 may be reduced to

$$\underline{C} = mt\, s_b \sqrt{2}\ \frac{1}{n_b} \qquad \text{II-39}$$

If $n_s = n_b = 1$, then Equation II-39 reduces to

$$\underline{C} = \sqrt{2}\, mt\ \ s_b \qquad \text{II-40}$$

In the majority of previous studies [72], the limit of detection is defined as that concentration or amount which will give a signal-to-noise ratio of 2 or 3. If the only major random errors are electrical and optical noises, then the rms noise is defined as approximately peak-to-peak noise divided by 5 [73]; thus, the limit of detection, $\underline{C}$, may be evaluated from Equation II-39, where $n_b = 5$ and $t = 3$, which gives a confidence level of better than 95 per cent.

CHAPTER III

EXPERIMENTAL

Reagents

Stock solutions were prepared from analytical reagent grade chemicals of $Pb(NO_3)_2$, $Na_2TeO_4 \cdot 2H_2O$, $AgNO_3$, Tl_2SO_4, and K $SbOC_4H_4O_6 \cdot \frac{1}{2} H_2O$ dissolved in deionized water to give concentrations of 10^3 $\mu g ml^{-1}$. Analytical reagent grade chemicals of SnO, MgO, and ZnO were dissolved in HCl and Zn metal, Co metal, and CdO were dissolved in HNO_3 and then diluted to 10^3 $\mu g ml^{-1}$. With concentrations varying by about a factor of 3, serial dilutions were performed with deionized water for concentrations ranging from 3×10^2 $\mu g ml^{-1}$ to the concentration resulting in a signal of 2 times peak-to-peak noise.

General Layout of the Experimental System

A schematic diagram of the experimental components in the atomic fluorescence system is shown in Figure 6. The components of this system are discussed below.

Sources of Excitation

Single-element electrodeless discharge lamps (EDL's) were prepared from the iodide form of the elements of Co,

Fig. 6.--Schematic diagram of continuous- and pulsed-sample introduction tube furnace atomic fluorescence spectrometric system.

E - Electrodeless discharge lamp (EDL).

B - Microwave power supply for EDL.

L_1, L_2, L_3 - Lenses.

S_1, S_2 - Apertures.

C - Chopper.

F - Vitreous carbon tube furnace.

M - Monochromator.

P - Photomultiplier tube.

V - High voltage power supply.

A - Preamplifier.

L - Lock-in amplifier.

R - Recorder readout.

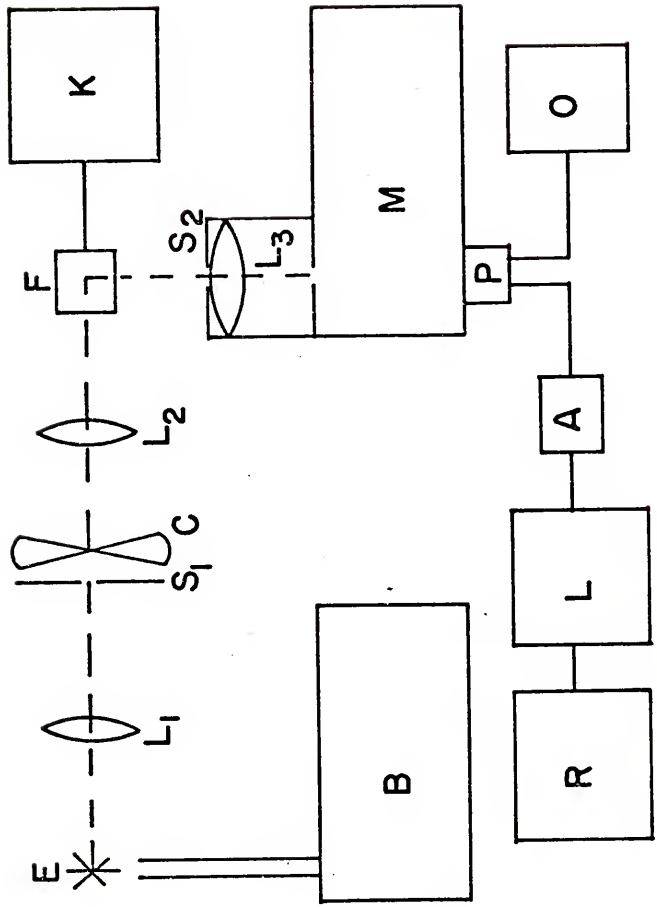
K
F
L
S2
L3
M
O
P
A
L2
S1
C
L1
L
E
B
R

Sn, Sb, Te, Pb, and Bi. The elements Ag, Tl, and Mg were prepared in their chloride form, while Zn and Cd were prepared in pure form as single-element EDL's. These EDL's were operated in the thermostated mode described by R. F. Browner et al. [74,75]. The apparatus used for thermostating the EDL's is shown in Figure 7. It consisted of a fan (Model NTH2, Rotron Mfg. Co., Woodstock, N.Y.) which blew room air over a heater coil (Model HG 751, Master Appliance Corp., Racine, Wis.) whose temperature was controlled with a laboratory Variac (Model 2 PF 1010, Staco, Inc., Dayton, Ohio). The temperature was monitored with a chromel-alumel thermocouple placed as shown in the metal conduit with temperature (°C) indicated directly on a voltmeter calibrated in temperature units (Model K, Barber-Coleman Co., Rockford, Ill.). The thermocouple was calibrated up to 350°C with a common laboratory thermometer, and because the temperature was in error by only 5 °C at 350°C and the error increased linearly with temperature, the error was extrapolated up to the maximum temperature used and then was corrected for. A change in 20 °C had very little effect (less than 5 per cent) upon the intensity of the EDL's when the EDL temperature was optimized.

The EDL was situated, as shown in Figure 7, in a microwave field focused with an "A" antenna. The EDL was powered by a microwave power generator (Model PGM-10,

Fig. 7.--Cutaway view of the EDL thermostating unit.
All brass construction.

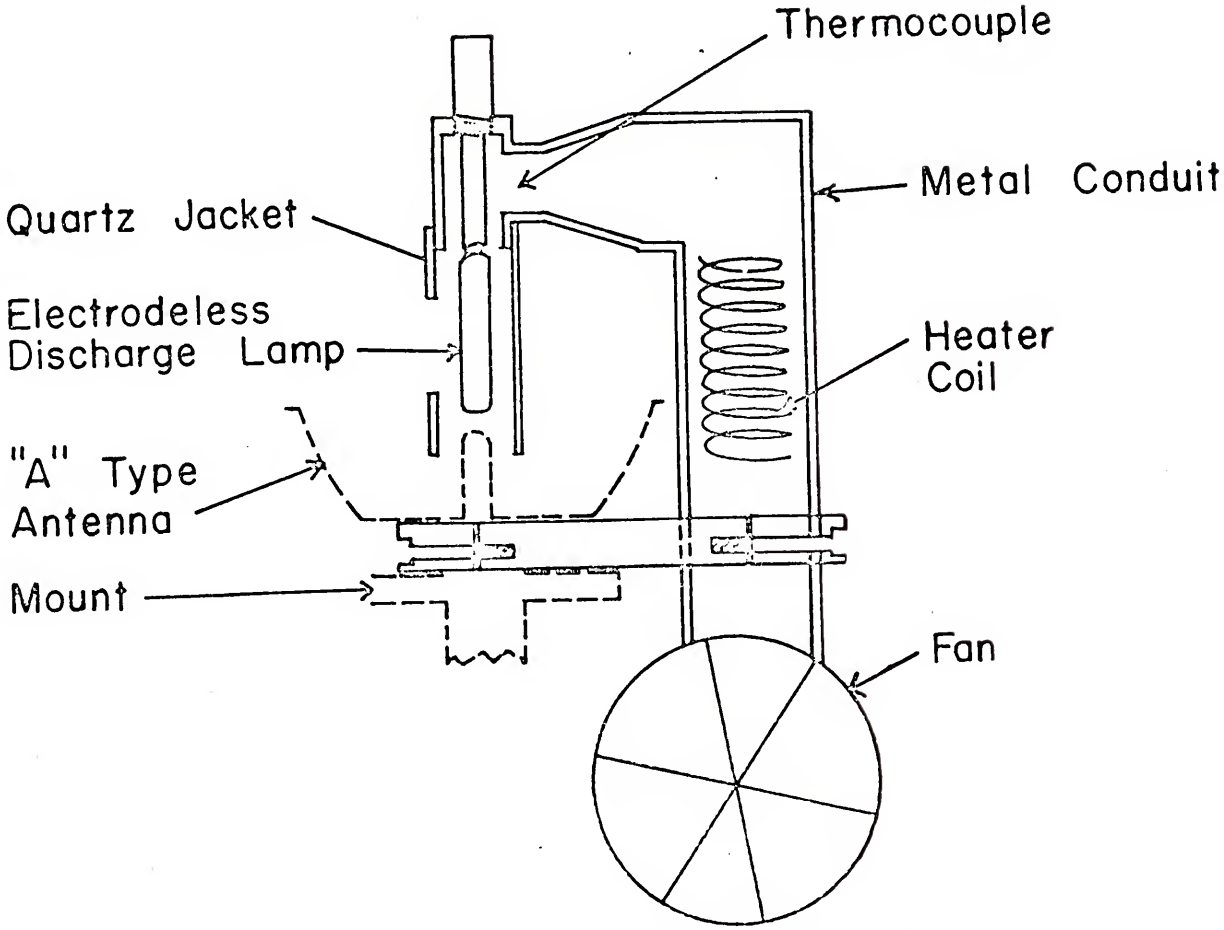
Thermocouple
Metal Conduit
Quartz Jacket
Electrodeless
Discharge Lamp
Heater
Coil
"A" Type
Antenna
Mount
Fan

Raytheon Co., Manchester, N. H.). The thermostated unit shown in Figure 7 from the bottom of the "A" antenna up was enclosed in an aluminum box measuring 4.5 in. wide, 7.0 in. long, and 6.0 in. high, with a hinged lid to facilitate changing EDL's. A 0.25 in. diameter hole was placed in a convenient location for the thermocouple to enter and a 1 in. diameter hole was located in such a position that the EDL radiation could be easily focused through the lenses upon the atom cell. When operating this unit at high temperatures (greater than 300 °C) (Model SP2A2, Rotron Mfg. Co.), a fan was needed to cool the microwave cable at the "A" antenna junction. The whole unit was mounted on two micrometer screw threads which gave both vertical and lateral adjustment to better than 0.1 mm to facilitate focusing the desired portion of the EDL upon the atom cell.

The single-element EDL's for these studies were operated at the temperatures and powers for the continuous mode studies and pulsed mode studies shown in Tables 3 and 5, respectively. The optimum temperatures and powers were experimentally determined each time the EDL was started by

i. lighting the EDL at a power of 50 W;

ii. adjusting the monochromator to the approximate wavelength of interest using light reflected from the EDL to the photomultiplier tube;

iii. while monitoring the intensity on a strip chart recorder, slowly raising the temperature of the EDL until the EDL intensity started to decrease from the maximum;

iv. decreasing the temperature until the maximum EDL intensity was attained;

v. fine tuning the wavelength;

vi. adjusting the microwave power to a reasonable (an increase in EDL intensity of 2-fold per 10 W power) trade off between high power and EDL intensity (high microwave power will decrease the EDL lifetime).

The EDL's for all but two elements were operated satisfactorily in this manner. However, the Sn and Mg EDL's needed a microwave power of 90 to 100 W (with temperature programming) to remain lit, and the optimum intensities were very sensitive to small changes in microwave power. This latter point was especially true for Mg; with moderate microwave power (50 W) the Mg EDL discharge was contained in only a small portion of the EDL volume. Even at 100 W, the discharge still did not fill the EDL cavity. In addition, several of the EDL's could be seen to fluctuate in intensity by the naked eye (through UV absorbing safety glasses, of course). An increase of microwave power usually eliminated this problem.

Optical System

Optical grade biconvex quartz lenses with a focal length of 2.5 in. and a diameter of 2 in. (Esco Products, Oak Ridge, N. J.) were used throughout for focusing. They were mounted on a steel plate with the aid of magnetic mounts (Model M 8-1, Enco Manufacturing Co., Chicago, Ill.)

and were aligned both vertically and horizontally with a He-Ne lab laser (Model ML 6805, Metrologic, Bellmaur, N. J.). For all absorption measurements performed, all three lenses were aligned to 180° with the entrance optics of the monochromator in such a manner that a 1:1 image was created at all focal points as checked with a tungsten filament lamp, and in such a way that the monochromator's mirrors and the diffraction grating were totally illuminated. For AFS measurements, the two lenses farthest from the monochromator were aligned vertically and horizontally so that the total solid angle of source intensity which impinged on the atom cell could be converted to useful fluorescence, as shown in Figure 6. Aperture S_1 of Figure 6 was 0.5 cm by 1 cm, so that all useful fluorescence from the atom cell would totally fill the slit width and height of the monochromator, and as mentioned previously, its mirrors and gratings. Aperture S_2 of Figure 6, was adjusted so that the collected fluorescence would just fill the solid angle of the monochromator and also fill all of its related optics. All measurements were performed with a 0.35 m f/6.8 Czerny-Turner monochromator (Model EU-700/E, Heath Co., Benton Harbor, Mich.).

Electronics

The electronic equipment used in these studies is also shown in Figure 6. The associated electronics included an RCA 1P28 photomultiplier powered by a high voltage power supply (Model EU-42A, Heath Co.), a lock-in amplifier tuned to 667 Hz (Model 391, Ithaco, Inc., Ithaca, N. Y.), and a preamplifier with variable gain (Model 164, Ithaco, Inc.). Source modulation was performed with a mechanical chopper (Model 382, Ithaco, Inc.), and the lock-in output was recorded on a potentiometric recorder (Model S. R., Sargent Welch Scientific Co., Skokie, Ill.).

Nebulizers

Different means of creating a wet aerosol mist from a solution have been used for atomic spectroscopy. Spinning disks, high voltage sparks, ultrasonic radiation, and pneumatic devices have all been employed to create these mists; however, only the latter two have received widespread attention in atomic spectroscopy. Of these, pneumatic nebulizers have been the commercially accepted choice because they have been inexpensive, sturdy, and reliable. However, they have suffered from the problems of creating a dispersed mist with widely varying particle diameters, and, when coupled to a spray chamber, poor aspiration efficiency; furthermore, they needed high gas flow rates to aspirate

properly, and were reported to have a maximum aerosol density of 0.03 g of solution/liter of aspiration gas [1,76].

Ultrasonic nebulizers have been plagued with various problems such as memory effects and sample transport capillary failure, and so were not used in these studies [76,77, 78]. Such nebulizers, however, function on very low flow rates of gas and hence result in relatively large solution-to-gas flow ratios. For further information on nebulization techniques, the reader is referred to the atomic spectroscopy review by Winefordner and Vickers [55].

In the present work, it was desired to build a high pressure, low sample consumption nebulizer using low flow rates of aspiration gas, although some difficulties were reported by other workers [1,79]. Such a nebulizer seemed to be ideally suited to non-flame AAS and AFS work. First, a miniaturized standard conical design similar to the one used in pneumatic nebulizers was used with limited success because the sample transport needle (id 0.003 in.) repeatedly plugged up. The original design was then slightly altered to that of nebulizer I, shown in Figure 8. The sample transport needle (I) used was a 6-in.-long 26 g stainless steel hypodermic needle (Hamilton Co., Reno, Nev.). This needle was strengthened by placing a concentric stainless steel tube around the exterior of the capillary needle, 0.5 in. from the tip until an outside diameter of 0.032 in. was

Fig. 8.--Schematic diagram of nebulizer I.

A - Nebulizer cone.
B - Rubber O-ring.
C - O-Ring seating gland.
D - Alignment rod.
E - Micrometer adjustment.
F - Housing ring to hold micrometer.
G - Stainless steel needle housing.
H - Teflon centering sleeve.
I - Hypodermic needle.
J - Vertical adjustment plate.
K - Nebulizer housing.
L - Needle housing.
M - Luer lock-luer lock connector.
N - Teflon system seal.
O - Retaining screw for N.

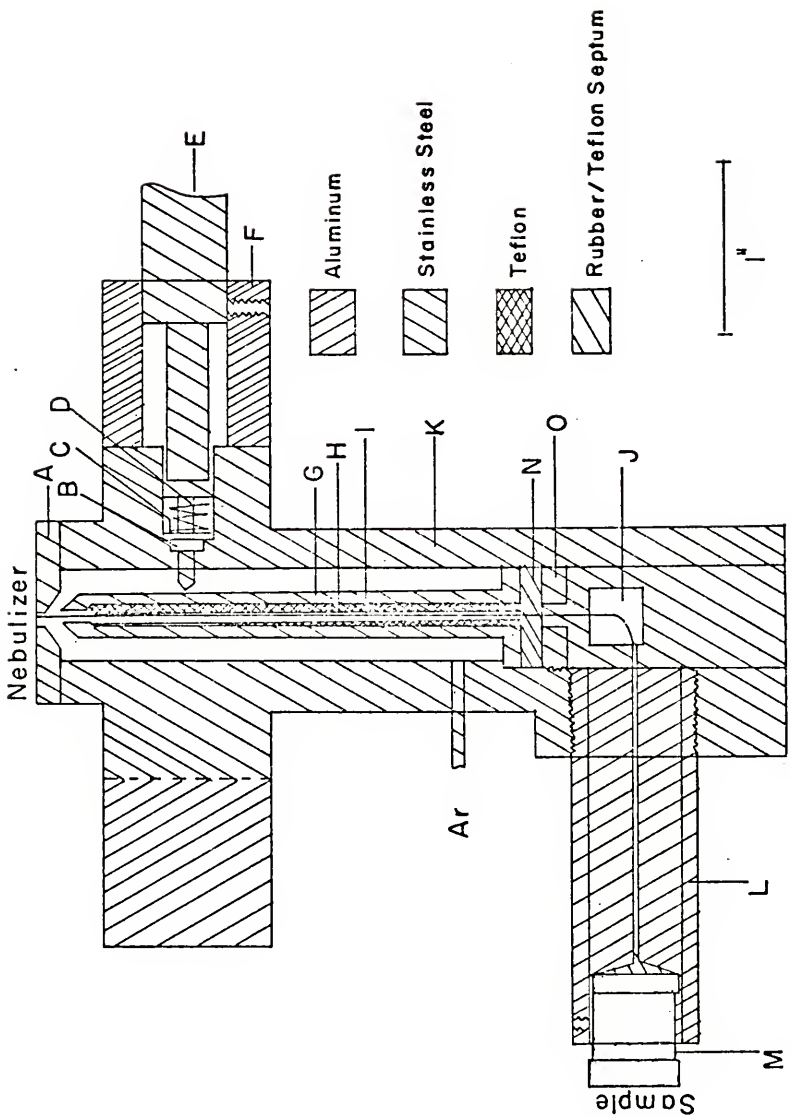
Nebulizer
A
B
C
D
E
F
G
H
I
K
N
O
J
L
M
Ar
Sample
Aluminum
Stainless Steel
Teflon
Rubber/Teflon Septum
1"

attained. This needle was held firmly in place in the stainless steel needle housing (F) with the use of a slip-fit Teflon centering sleeve (H). The transport needle was epoxied in place to the retaining screw (O) for the Teflon system seal (N). The nebulizer cone was machined to have a 0.020 in. inside diameter and a convergence angle of the aspirating gas nozzle to the central solution capillary of 30°. This left a clearance of 0.001 in. between the solution capillary and the aspirating gas nozzle when the former was centered. The centering of the sample transport needle was effected with three stainless steel micrometers which were situated at 120° about the needle with the aid of a 30 power microscope (Model 70, 266, Edmund Scientific Co., Barrington, N. J.). In the continuous-sampling studies, sample solution was force-fed through the sample transport needle with the aid of a syringe pump (Model 353, Sage Instruments, Inc., White Plains, N. Y.).

Nebulizer II was designed for use in both the continuous- and the pulsed-sampling modes. Nebulizer I contained a dead volume of greater than 0.120 ml between the syringe and the exit of the sample transport needle, which caused very severe memory effects when sampling in the pulsed mode. The dead volume was reduced by shortening the sample transport needle to 2 in. in length, eliminating the Luer-lock luer-lock connection by epoxying and crimping a

male unit to the Teflon tubing, and decreasing the length of the Teflon tubing from 12 in. to 6 in. The former change necessitated the complete redesign of the nebulizer housing and sample transport needle centering apparatus; however, critical aspiration parameters were not altered, such as the 30° convergence angle of the aspirating gas nozzle to the central solution capillary and the clearance between the solution capillary and aspirating gas nozzle of 0.001 in. Nebulizer II is shown in Figure 9. The overall dimensions of the nebulizer were 1.375 in. in diameter and 2 in. in length. 10-80 Stainless steel screws (D) were situated at 120° around the hypodermic needle to allow centering of the hypodermic needle (H) in the aspirating gas nozzle (A).

All other parts, as mentioned previously, functioned similarly to the parts of nebulizer I, shown in Figure 8, and will not be discussed further.

Desolvation Chamber

A desolvation chamber, heated with heating tape (Samox Hi Temperature Tape, Arthur H. Thomas Co., Philadelphia, Pa.), connected the nebulizer with the vitreous carbon non-flame cell. Desolvation chambers constructed of quartz and glass were found unsatisfactory, due to inability to form a simple, efficient, gas-tight seal between the

Fig. 9.--Schematic diagram of nebulizer II.

A - Nebulizer cone.

B - Rubber O-ring.

C - Rubber O-ring retaining screw for B.

D - Alignment screw.

E - Nebulizer housing.

F - Stainless steel needle housing.

G - Teflon centering sleeve.

H - Hypodermic needle.

I - Teflon system seal.

J - Retaining plate for I.

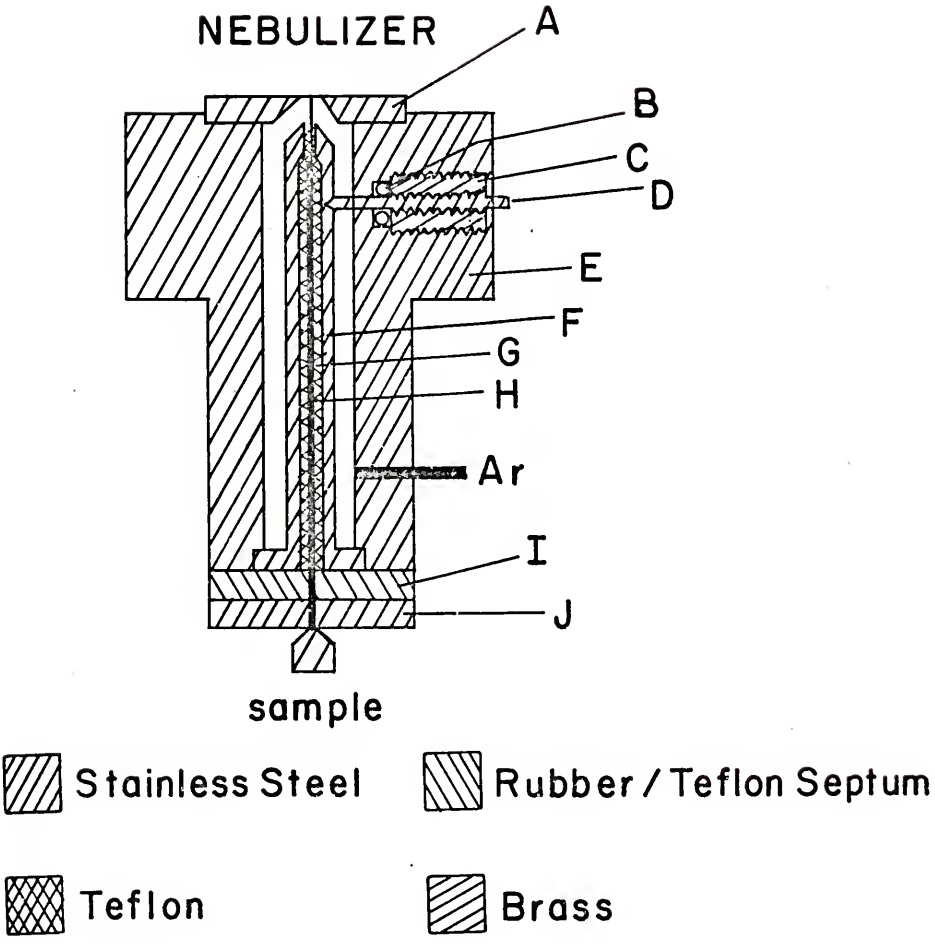
NEBULIZER
A
B
C
D
E
F
G
H
Ar
I
J
sample
Stainless Steel
Rubber / Teflon Septum
Teflon
Brass

chamber and the nebulizer. Without a good seal, repetitive pulsed atomic fluorescence signals were obtained while sampling in the continuous mode. Thus, the desolvation chamber shown in Figure 10 was machined from type 304 stainless steel. It was bolted to the top of the nebulizer with sheet asbestos serving as a gasket and, to some extent, as a thermal insulation for the nebulizer. The desolvation chamber had an inside diameter of 1.375 in. and was 3.5 in. long. The top inside of the desolvation chamber was reduced to a radius of 0.688 in. The male unit of the desolvation chamber was tapered from 0.297 in. outside diameter at the top to 0.313 in. outside diameter at the base to facilitate forming a leak-proof seal to the vitreous carbon tube furnace. Around the inside rim at the base of the desolvation chamber were entrance ports to add other gases than were used to effect nebulization.

Vitreous Carbon Tube Furnace

The vitreous carbon tube furnace is shown in Figure 11. Its outside dimensions are 2.5 in. wide by 2.5 in. long and 2.0 in. in height. All parts ultimately connect to the water-cooled main brass furnace housing (F). Both top and bottom water-cooled electrodes (B) contained a copper slide (A) to facilitate electrical contact. The top water-cooled copper electrode (B) had three concentric

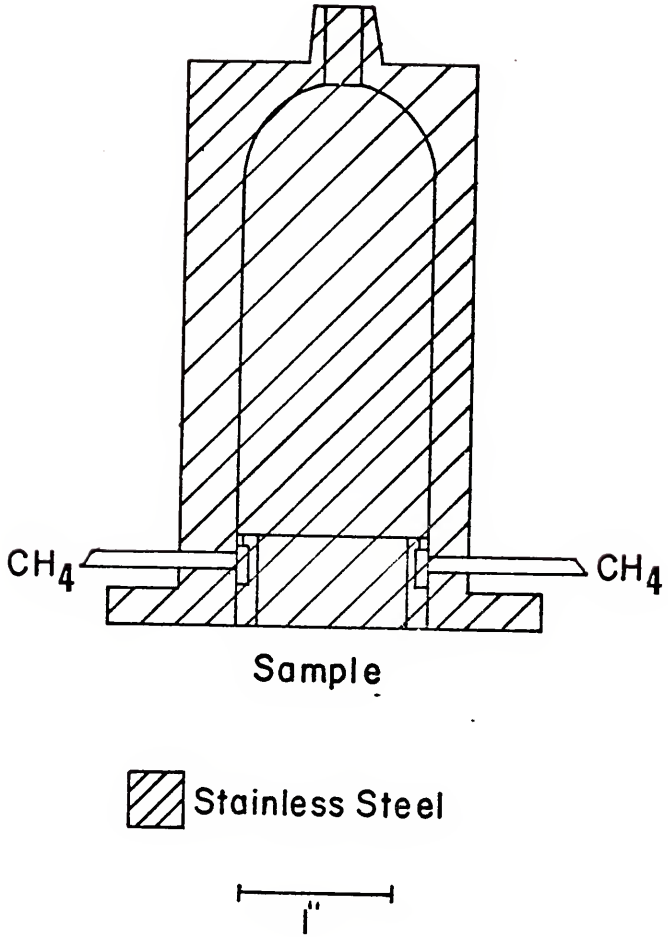

Fig. 10.--Schematic diagram of the stainless steel desolvation chamber.

Fig. 11.--Schematic diagram of vitreous carbon tube furnace.

A - Copper electrical contacts.

B - Water-cooled electrodes.

C - Vitreous carbon tube.

D - Boron nitride insulation ring.

E - Asbestos insulation ring.

F - Furnace housing.

G - Graphite rings for electrical contact.

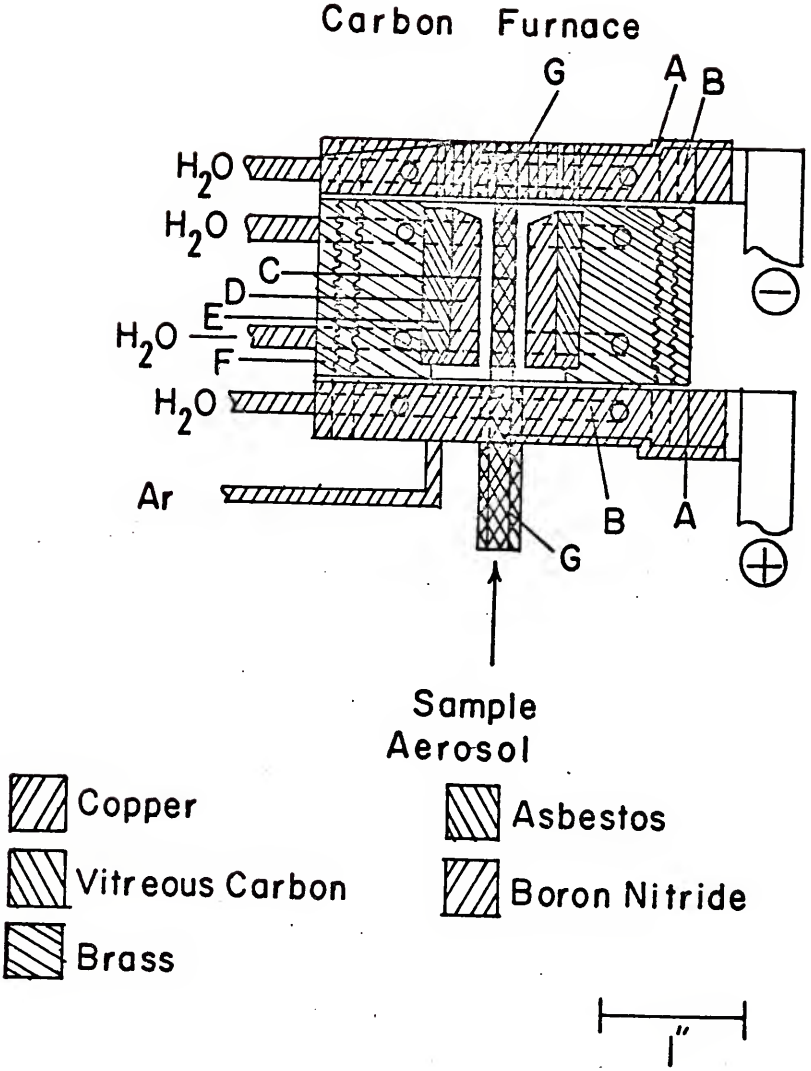
Carbon Furnace
G
A
B
H_2O
H_2O
C
D
E
H_2O
F
H_2O
Ar
B
A
G
Sample
Aerosol
Copper
Asbestos
Vitreous Carbon
Boron Nitride
Brass
1"

circular arrays of holes (used for inert sheath gases) of 1 mm in diameter at radii from the center of the vitreous carbon tube of 13 mm, 17 mm, and 19 mm, respectively. These holes were staggered with each other to minimize O_2 and N_2 entrainment from the air. The two main electrodes (B) were electrically insulated from the brass furnace housing (F) with fiberglass gaskets and nylon screws (the external surface of the furnace housing was less than 75 °C when the vitreous carbon tube (C) was operating at temperatures in excess of 2000 °C). Thermal insulation was provided with rings of boron nitride (D) and asbestos (E) between the vitreous carbon tube furnace (C) and the furnace housing (F).

Perhaps the most critical tolerances in this furnace are the inside diameters and outside diameters of the upper and lower graphite rings (G), providing electrical contact, as well as the thickness of the upper graphite ring (G). If the rings (G) were not machined to have a snug slip fit to the vitreous carbon tube (C), the electrical resistance became so great that the maximum voltage (20 V) from the power supply (SCR 20-250, Electronics Measurements, Neptune, N. J.) could not supply enough current to sufficiently heat the carbon tube. The thickness of the upper graphite ring (G) determined the resistance of the contact between it and the vitreous carbon tube (C), and hence the power dissipated

near the atom cell. (It thus was used to influence the temperature of not only the vitreous carbon furnace, but also the atom cell.) The lower graphite ring (G) had an orifice of 0.297 in. in diameter to accept the previously mentioned male unit of the desolvation chamber.

Nebulizer, Desolvation Chamber, and Vitreous Carbon Tube Furnace Mount

The nebulizer and vitreous carbon tube furnace were mounted on a 0.5 in. thick, by 2.0 in. wide by 12.5 in. long piece of aluminum in such a manner that the former, with the desolvation chamber in place, could easily be moved up or down 5 in. and locked in place while the vitreous carbon tube furnace was kept fixed. This whole assembly was mounted on two micrometer screw threads which gave both vertical and horizontal adjustment to better than 0.1 mm to facilitate imaging the atom cell upon the monochromator entrance slit.

Procedure for Evaluation of Experimental Characteristics of the System

Gas flow rates

The rotameters were calibrated for various gas flow rates at different pressures. These calibrations are given in Appendix II.

Sample solution flow rates

Flow rates, using the syringe pump and 1 ml disposable tuberculin syringes (Model 501 S-TB, Sherwood Medical Industries, Inc., Deland, Fla.), to pump the sample through the nebulizer, were calibrated versus the coarse flow rate scale and the percentage flow rate scale of the syringe pump. The aerosol produced was of a pulsed nature when samples with very low flow rates were aspirated with an Ar flow rate of 0.90 l min^{-1}. These results are summarized in Table 1. A flow rate of 0.12 ml min^{-1} was chosen as a nominal sample flow rate for all measurements.

Mean particle diameter

The mean particle diameter of the wet aerosol formed upon aspiration may be estimated from the empirical equation which Nukiyama and Tanasawa determined for velocities up to sonic velocities for a conical pneumatic nebulizer [1]. Their equation for the mean particle diameter, d, in un was

$$d = \frac{585}{v}\left(\frac{\sigma}{\rho}\right)^{1/2} + 597\left[\frac{\eta}{(\sigma\rho)^{1/2}}\right]^{0.45}\left[1000\,\frac{V_l}{V_a}\right]^{1.5} \qquad \text{III-1}$$

where

TABLE 1

STABILITY[a] OF AEROSOL PRODUCTION WITH HIGH PRESSURE NEBULIZER

Sample Flow Rate (ml min^{-1})	Ar Flow Rate Nebulizer (l min^{-1})	Stability of Aspiration
0.50	0.90	yes
0.25	0.90	yes
0.12	0.90	yes[b]
0.06	0.90	yes[b]
0.03	0.90	no[c]
0.25	0.78	yes
0.12	0.78	yes
0.06	0.78	yes[b]

[a]Measured stability by monitoring light scattered from aerosol droplets emerging from nebulizer.

[b]After a time delay of 10 sec.

[c]No = stability of aspiration was inadequate for analytical work.

ν = velocity of aspiration gas

σ = surface tension

ρ = density of liquid

V_l = volume of liquid (l)

V_a = volume of aspiration gas (l)

η = viscosity

It should be noted that if $V_a = 5000\ V_l$, then for water, the Nukiyama and Tanasawa equation (Equation III-1) reduces to [1]

$$c = \frac{585}{\nu} \left(\frac{\sigma}{\rho}\right)^{1/2} \qquad \text{III-2}$$

The velocity of the aspiration gas through the nebulization cone was estimated by dividing the measured flow rate of the aspiration gas by the area of the ring-shaped orifice. The value calculated in this manner was 390 m sec^{-1} for an aspiration flow rate of 0.90 l min^{-1}. Substituting the speed of sound, 340 m sec^{-1}, for ν in Equation III-2, a mean particle diameter of 15 μm was calculated. The calculated velocity of approximately 10 per cent greater than the speed of sound would further increase turbulence and hence, tend to decrease the particle size even more.

Desolvation time

The aerosol mist was dispersed and desolvated in the stainless steel desolvation chamber previously described. The temperature of the gas passing through the center of

the desolvation chamber ranged from 246 °C to 278 °C as shown in Figure 12, while the heat tape wrapped around the chamber was measured at 393 °C. These temperatures were measured with 0.015 in. diameter chromel-alumel thermocouples, and the resulting voltages were monitored on a digital multimeter (Model 414, Dynasciences, Chatsworth, Cal.).

Desolvation time, t, of a particle may be approximated with the following equation [80].

$$t_s = \frac{A_o C_p / \pi \lambda}{\ln[1 + C_p(T-T_b)/L]} \qquad \text{III-3}$$

where

t_s = desolvation time (sec)

ρ = density of the liquid (g cm^{-3})

A_o = initial area of the droplet (cm^2)

C_p = specific heat of the vapor (cal $g^{-1}°C^{-1}$)

λ = thermal conductivity of the gas (cal sec^{-1} $cm^{-1}°C^{-1}$)

T = desolvation temperature (°C)

T_b = boiling point of the solvent (°C)

L = specific heat of vaporization of the solvent (cal g^{-1})

This equation neglects the additional transport of heat to the boiling droplet by convection, which would significantly reduce the actual desolvation time. Using Equation III-3, a desolvation time of 23 msec for a 15 μm diameter sphere

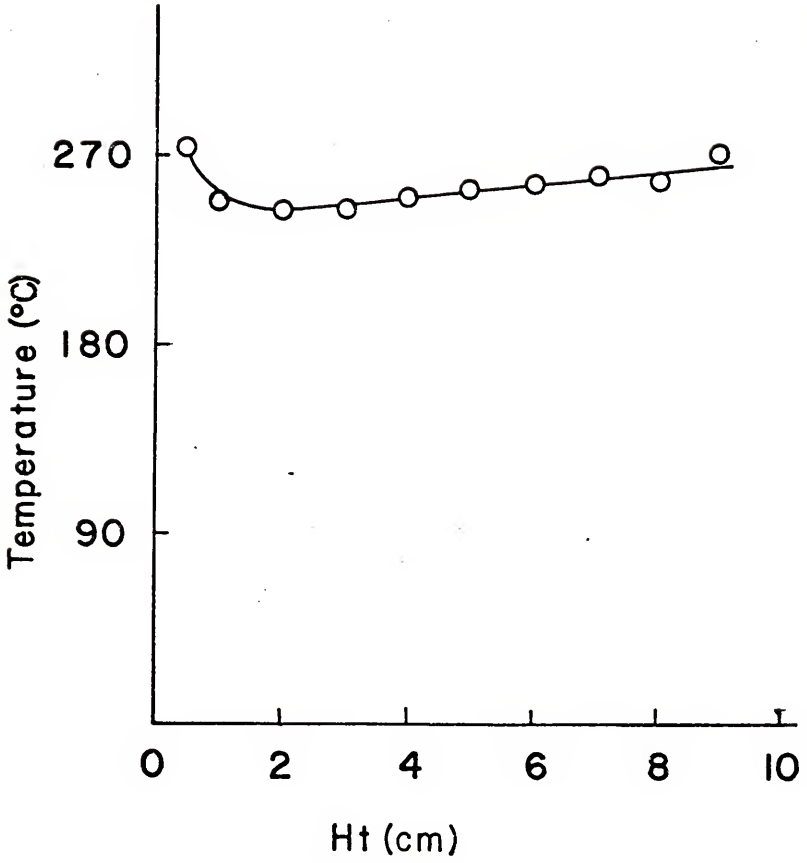

Fig. 12.--Gas temperatures in the desolvation chamber at various heights above the nebulizer.

of water at 250 °C was calculated. Also, from the known nebulization gas flow rate and the volume of the desolvation chamber, a residency time of the sample mist in the desolvation chamber of 5.3 sec was calculated, neglecting the additional gaseous volume of the liquid sample solution. Thus, desolvation was probably completed in the desolvation chamber.

Scattered radiation

No scattered radiation (in the absorption mode) was discernible from water or from a 100 $\mu g\ ml^{-1}$ Zr solution at the Zn 213.8 nm line which was radiated from a Zn hollow cathode while absorption measurements were being made at grazing incidence to the desolvation chamber. The scatter signal was found to be 2 per cent absorption for scatter measurements performed with 10^4 $\mu g\ ml^{-1}$ Zr [81]. The negligible amount of scatter from large concentrations of solutes, which are difficult to vaporize, qualitatively supports the above observations concerning the small mean particle diameter.

Rise velocities

Comparisons of the rise velocities in the vitreous carbon tube non-flame to that in various analytical premixed flames (assuming a primary combustion zone angle of 6°) are given in Table 2 [1]. Ratios of the residency time in the

TABLE 2

COMPARISON OF RESIDENCY TIMES IN ATOM CELLS

Rise Velocity[a] ($m\ sec^{-1}$)	
C-furnace	0.8
H_2-O_2	20.
H_2-air	0.4
C_2H_2-O_2	20.
C_2H_2-air	2.
C_2H_2-N_2O	1.6

Residency Time Ratios[b]	
C-furnace:H_2-O_2	50:1
C-furnace:H_2-air	1:1
C-furnace:C_2H_2-O_2	50:1
C-furnace:C_2H_2-air	5:1
C-furnace:C_2H_2-N_2O	4:1

[a]Rise velocities for the flames were calculated from $v_{burn} = r_{rise} \sin \theta$, where v_{burn} is the burning velocity (taken from Reference 1).

[b]Residency time was calculated from $t_R = \frac{h_o}{r_{rise}}$, where h_o for the flames is the observation height above the burner taken to be 2.5 cm and h_o for the furnace was taken to be the tube length of 5 cm.

vitreous carbon tube to the residency time in a flame prior to measurement (assuming a distance of 2.5 cm) are also given in Table 2.

Efficiency of sample transport

The efficiency of the nebulizer and desolvation chamber was experimentally determined by aspirating 2 ml of 12.5 $\mu g\ ml^{-1}$ Mg. The chamber was then washed with deionized water of the same pH as the original solution, and the Mg concentration of this solution was measured via atomic absorption spectrometry with the graphite filament non-flame cell [30]. The efficiency was found to be 93 per cent. The chamber was then rewashed in the same manner to check for any residual Mg, and no detectable Mg was found.

Temperature of furnace and gaseous vapor

The temperatures in and above the vitreous carbon tube resulting from various applied currents from a constant current source were measured with 0.010 in. diameter tungsten-tungsten 26 per cent rhenium thermocouples (Omega Engineering, Inc., Stamford, Conn.). The voltages were monitored on a digital multimeter (Model 414, Dynasciences). The results are given in Figure 13.

Fig. 13.--Temperatures of non-flame cell at various points.

a - Temperature in center of carbon tube.

b - Temperature at grazing incidence to carbon tube with Ar sheath.

c - Temperature at grazing incidence to carbon tube with Ar-H_2 diffusion flame.

d - Temperature at 1 cm above carbon tube with Ar-H_2 diffusion flame.

e - Temperature at 2 cm above carbon tube with Ar-H_2 diffusion flame.

f - Temperature at 1 cm above carbon tube with Ar sheath.

g - Temperature at 2 cm above carbon tube with Ar sheath.

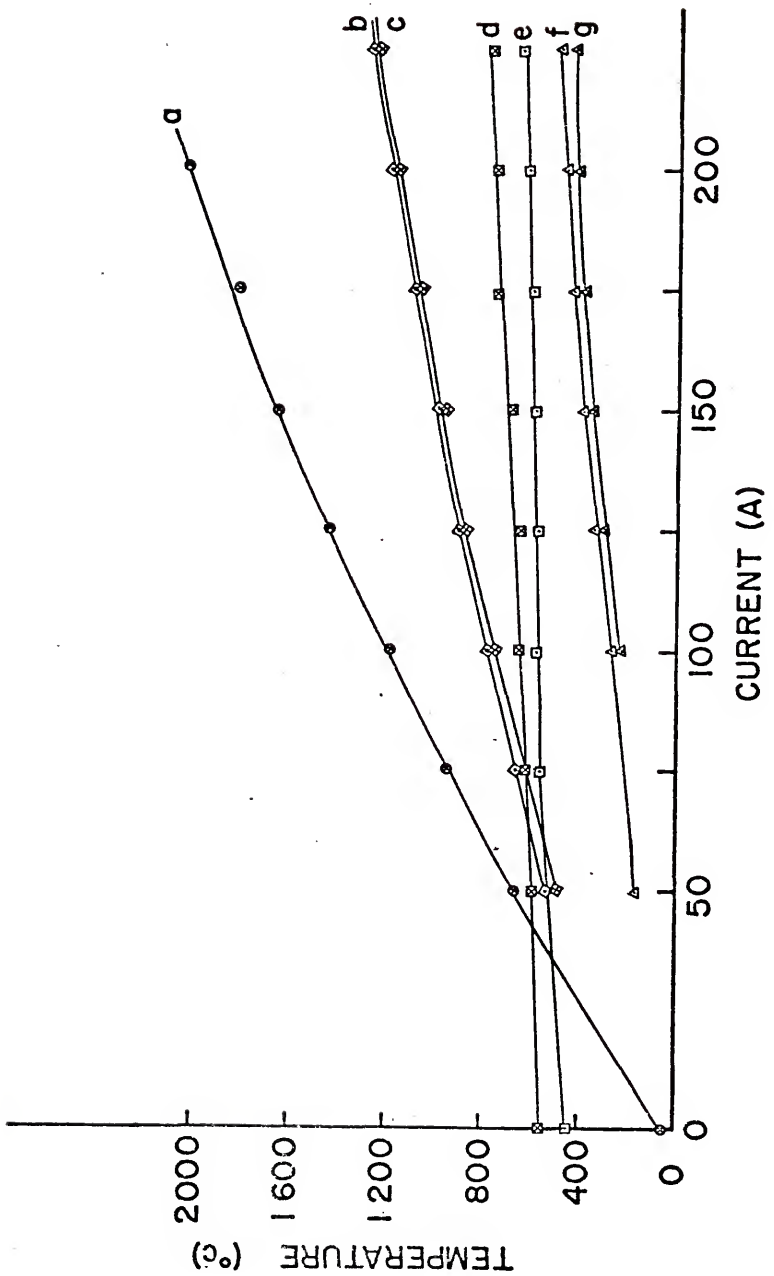
TEMPERATURE (°c)
2000
1600
1200
800
400
0
0
50
100
150
200
CURRENT (A)
a
b
c
d
e
f
g

General Procedure for Making Atomic Fluorescence Measurements

All electronic equipment (photomultiplier tube, lock-in amplifier, chopper, etc.) was switched on at least 30 minutes before any experimental data were recorded. The desolvation chamber required approximately 30 minutes to reach the steady state in temperature shown in Figure 12, while the EDL's usually required about 40 minutes to optimize.

The nebulizer, desolvation chamber, and vitreous carbon tube furnace were flushed with Ar for approximately 5 to 10 minutes before any atomic fluorescence measurements were performed. Increasing amounts of current were applied to the carbon tube furnace until the desired temperature was reached after the desired flow rates of Ar, H_2, and CH_4 were adjusted. The sample (or blank) was then aspirated into the desolvation chamber in either the pulsed or continuous modes of sampling, and the resulting aerosol mist was carried to the vitreous carbon tube where atomization was effected. The vitreous carbon furnace was operated at a constant current (temperature) until all atomic fluorescence measurements were completed.

The continuous mode of sampling was achieved by force-feeding the solution to the high pressure nebulizer with a syringe pump (Model 353, Sage Instruments), while the pulsed mode was effected by forcing the sample into the

nebulizer operated continuously at 60 pounds pressure of Ar from a 0.5 ml syringe (Model 1000, Hamilton Co.) contained in a repeating dispenser (Model PB-600, Hamilton Co.).

The excitation radiation passed at grazing incidence to the top of the vitreous carbon tube. The fluorescence was collected by the monochromator adjusted to the desired wavelength. The slit width was adjusted to 750 μm for all studies. The Ar, CH_4, and H_2 flow rates (see Appendix II) were monitored by rotameters calibrated with a wet test meter (Model S-39447, Precision Scientific Co., Chicago, Ill.).

CHAPTER IV

RESULTS AND DISCUSSION

Atomic Fluorescence Signal-to-Noise Optimization

Five 1P28 photomultiplier tubes were examined for both dark current and relative gain characteristics at various applied voltages (600 V - 900 V); the gain was determined with a tungsten filament lamp as the source operated at a constant voltage (intensity), a wavelength of 500 nm, and a slit width of 200 nm. The optimum photomultiplier tube (of the five measured) was used for all fluorescence measurements; at the voltage (700 V) found to give the optimum signal-to-noise ratio, a dark current of 1×10^{-10} A at 700 V was measured.

As mentioned in Chapter III, the intersection of the center of the excitation optics and the center of the emission optics (L_1 and L_2, L_3 and M, respectively of Figure 6) was determined; this intersection could be located to better than 1 mm using a removable marker. The vitreous carbon tube furnace alignment was coarsely adjusted in this manner, and then, using the vertical and horizontal screw adjusts, the fluorescence signal was finely tuned to a maximum.

Because ideally a fluorescence signal should be measured against no background signal, two apertures (S_1 and S_2 of Figure 6) were used to prevent most source radiation from being scattered about the room and eventually finding its way to the photomultiplier tube. Care was taken to ensure that the aperture did not limit the solid angle of the monochromator.

No mirrors were used to increase fluorescence intensity by reflecting the source intensity back upon the atom cell or in collecting a larger solid angle of the fluorescence radiation from the atom cell. An improvement of signal-to-noise (S/N) by a factor of 3-10 by employing mirrors for this purpose has been reported in atomic fluorescence flame spectroscopy [82].

The optimum time constant of the lock-in amplifier (resulting in optimum fluorescence S/N) used in the pulsed mode was experimentally determined for several elements and was found to be 0.4 sec.

Fluorescence signal-to-noise for a number of elements was determined at various monochromator slit widths, and a 750 μm slit appeared to be a suitable compromise choice for all elements.

On the average, about five EDL's for each element determined were characterized as to their optimum temperature range, operating power, long term lamp stability,

relative intensities at the wavelength of interest, and short term noise at the optimum temperature (intensity). These characteristics were determined as described previously in Chapter III. All results were recorded, and the respective lamps were labeled. The figures of merit for each EDL, for example, optimum temperature range, intensity, operating power, long term stability, and short term stability were checked for the particular lamp in use before any atomic fluorescence measurements were performed to determine if the lamp was still near optimum characteristics. If not, another EDL was used.

The atomic fluorescence signal-to-noise of Pb and Sn was examined for vitreous carbon tubes with internal diameters of 0.188 in. and 0.125 in. The S/N for the 0.188 in. tube was larger by approximately a factor of 2 for Pb and Sn than for the 0.125 in. tube. Therefore, it was used for all further atomic fluorescence measurements. The upper graphite ring for electrical connection (G of Figure 11) was changed in thickness to values of 0.050 in., 0.060 in., 0.080 in., and 0.100 in., and the resulting atomic fluorescence intensities were measured for Te, Pb, and Sn. A thickness of 0.080 in. gave the optimum S/N ratios when the vitreous carbon tube lifetime was taken into account, so this thickness was used for all further atomic fluorescence measurements.

The optimum temperatures of the vitreous carbon tube furnace were determined experimentally for each element by comparing fluorescence S/N ratios. The vitreous carbon tube lifetime was also taken into consideration here; higher temperatures led to shorter lifetimes of the vitreous carbon furnace.

The gas flow rates (nebulization Ar flow rate, external Ar flow rate, external H_2 flow rates, and internal CH_4 flow rates) were optimized for each respective element in the continuous mode study; however, in the pulsed mode study, average optimum flow rates for all elements were used. Internal Ar was also added for Ag, Pb, Sn, and Tl in the continuous mode of operation; however, in all cases, the fluorescence S/N ratio decreased markedly, and so it was not further examined. This may be the result of increased atom cloud dilution in the atom cell or decreased residency times of the analyte in the vitreous carbon tube furnace.

Definitions of Analytical Parameters

The atomic fluorescence concentration ($\mu g\ ml^{-1}$) limit of detection (CLOD) was defined as that concentration (in $\mu g\ ml^{-1}$) giving a signal of 3 x rms noise. Each LOD was found by alternately running a signal and blank 3-5 times and then extrapolating back from a signal of about

2 x peak-to-peak noise to a signal of 3 x rms noise and determining the concentration of the lowest signal level. Atomic fluorescence measurements of the various elements were determined for concentrations ranging from 10^3 $\mu g\ ml^{-1}$ to the concentration resulting in a signal of 2 x peak-to-peak noise with concentrations varying by factors of three. The upper concentration limit (called UCL) was determined by the beginning of serious curvature (greater than 4 per cent deviation from linearity) of the analytical curve. The linear dynamic range (LDR) was the ratio of UCL/LOD, and the sensitivity was the slope of the analytical curve. The precision of the system (relative standard deviation) was determined for a concentration of 100-200 x LOD.

Continuous-Sampling Mode Results

Limits of detection

The resulting LOD's for the six elements are given in Table 3, along with the temperature of atomization, various gas flow rates, and the linear dynamic ranges (LDR). The atomic fluorescence LOD's obtained by the present non-flame cell were compared to the best limits of detection obtained with a flame and a resistively heated discrete sampling non-flame cell in Table 4. Both concentration (in $\mu g\ ml^{-1}$) limits of detection (CLOD) and absolute (in ng) limits of detection (ALOD) are listed in Table 4. The

TABLE 3

EXPERIMENTAL CONDITIONS AND ANALYTICAL RESULTS FOR MEASUREMENT OF SEVERAL ELEMENTS BY MEANS OF THE CONTINUOUS-SAMPLE INTRODUCTION TUBE FURNACE ATOMIC FLUORESCENCE SPECTROMETRIC SYSTEM

Element	Wavelength (nm)	EDL Conditions		Tube Furnace Conditions				LOD[e] ($\mu g\ ml^{-1}$)	LDR[e]	RSD[f]	Sensitivity[g]
		Temp.[a] (°C)	Power[b] (W)	Temp.[c] (°C)	Ar Flow Rate Nebulizer ($l\ min^{-1}$)	Ar Flow Rate External ($l\ min^{-1}$)	H_2 Flow Rate[d] External ($l\ min^{-1}$)				
Te	214.2	430	30	1515	0.78	4.7	1.8	$1x10^{-2}$	$1x10^{4}$	0.048	0.87
Ag	328.0	530	60	1675	0.78	4.3	1.6	$2x10^{-3}$	$1.5x10^{3}$	0.035	0.98
Pb	283.3	430	30	1675	0.78	4.3	1.6	$1x10^{-2}$	$8x10^{3}$	0.032	1.0
Sn	303.4	275	90	1800	0.78	5.8	1.8	$1x10^{-2}$	$1x10^{3}$	0.045	1.3
Tl	377.6	435	45	1675	0.9	4.7	1.6	$6x10^{-3}$	$3x10^{3}$	0.036	1.0
Bi	307.7	500	50	1540	0.9	4.7	1.8	$2x10^{-3}$	$1x10^{4}$	0.015	0.96

[a] Temperature of air flowing by EDL.

[b] Microwave power applied to EDL using thermostated "A" antenna.

[c] Temperature of graphite tube furnace walls.

[d] Flow rate of Ar and/or H_2 around tube furnace exit.

[e] LOD = limit of detection (see text for definition).
LDR = linear dynamic range (see text for definition).

[f] RSD = relative standard deviation (taken at a concentration of about 100xLOD).

[g] Sensitivity = slope of Log-Log plots.

TABLE 4

COMPARISON OF NON-FLAME ATOMIZATION ATOMIC FLUORESCENCE SPECTROMETRIC LIMITS OF DETECTION

Element	This Work CLOD ($\mu g\ ml^{-1}$)	This Work ALOD (ng)	Discrete Atomization CLOD ($\mu g\ ml^{-1}$)	Discrete Atomization ALOD (ng)	Ref.	Flame CLOD ($\mu g\ ml^{-1}$)	Flame ALOD (ng)	Ref.
Sn	$1x10^{-2}$	$1x10^{0}$	$2x10^{-1}$	$1x10^{-1}$	33	$1x10^{-1}$	$5x10^{2}$	83
Pb	$5x10^{-3}$	$5x10^{-1}$	$5x10^{-3}$	$3x10^{-3}$	36	$1x10^{-2}$	$5x10^{1}$	84
Te	$1x10^{-2}$	$1x10^{0}$	-	-	-	$6x10^{-3}$	$3x10^{1}$	85
Ag	$2x10^{-4}$	$2x10^{-2}$	$8x10^{-4}$	$4x10^{-4}$	33	$1x10^{-4}$	$5x10^{-1}$	86
Tl	$6x10^{-3}$	$7x10^{-1}$	$4x10^{-2}$	$2x10^{-2}$	33	$8x10^{-3}$	4x10	86
Bi	$2x10^{-3}$	$2x10^{-1}$	-	-	-	$5x10^{-3}$	2x10	85

flame atomic fluorescence ALOD was approximated by assuming that measurements were performed for 1 minute with a sample flow rate of 5 ml min^{-1}.

In general, the present system operated in the continuous mode resulted in concentration limits of detection which did not vary significantly from those concentration limits of detection found by flame and non-flame atomic fluorescence. The absolute limits of detection of the present system operated in the continuous mode were generally 1-2 orders of magnitude better than flame atomic fluorescent limits of detection, but about 1 order of magnitude poorer (higher) than filament non-flame atomic fluorescence spectroscopy.

Linear dynamic range and sensitivity

The atomic fluorescence analytical curves for Te, Sn, Ag, Bi, Pb, and Tl with the present vitreous carbon tube in the continuous-sampling mode are given in Figures 14, 15, 16, 17, 18 and 19, respectively. The linear dynamic ranges varied from 1 x 10^3 for Sn to 1.5 to 10^4 for Bi, and are listed in Table 4. Bi has a slightly concave analytical curve; however, it is certainly analytically useful. The discrete sampling filament non-flame cell, when measurements were performed by atomic fluorescence spectroscopy, appears to have significantly shorter linear dynamic ranges (1 x 10^2 - 5 x 10^3) for a number of elements investigated [34].

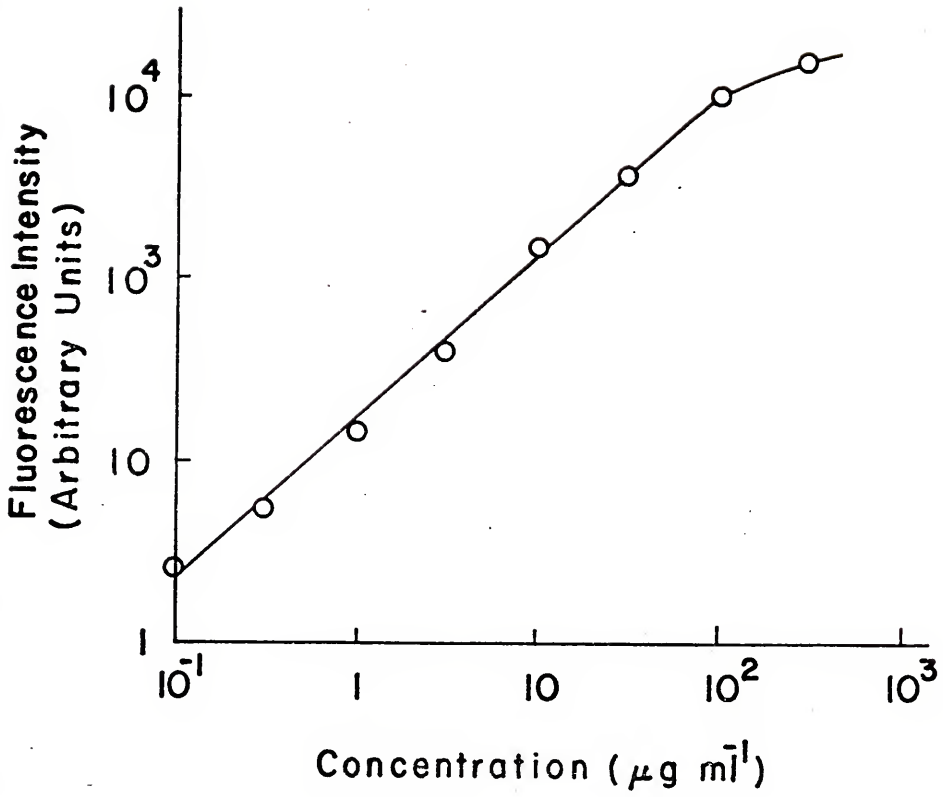

Fig. 14.--Atomic fluorescence analytical curve for Te in the continuous mode of operation.

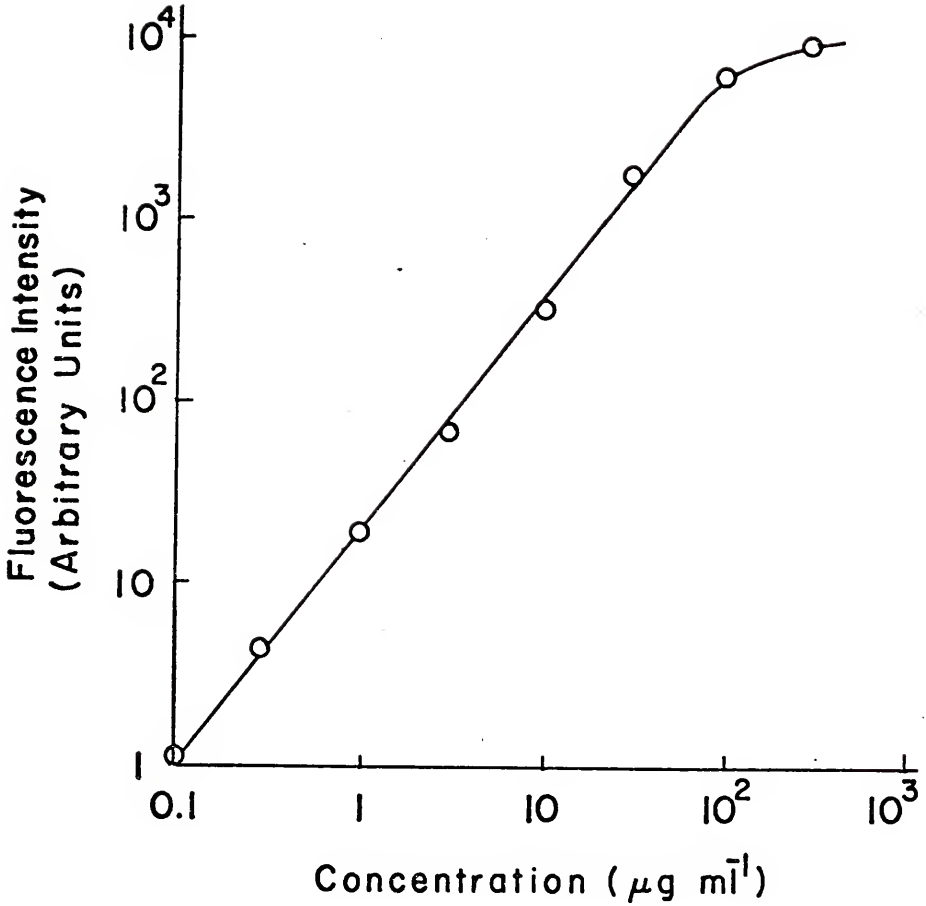

Fig. 15.--Atomic fluorescence analytical curve for Sn in the continuous mode of operation.

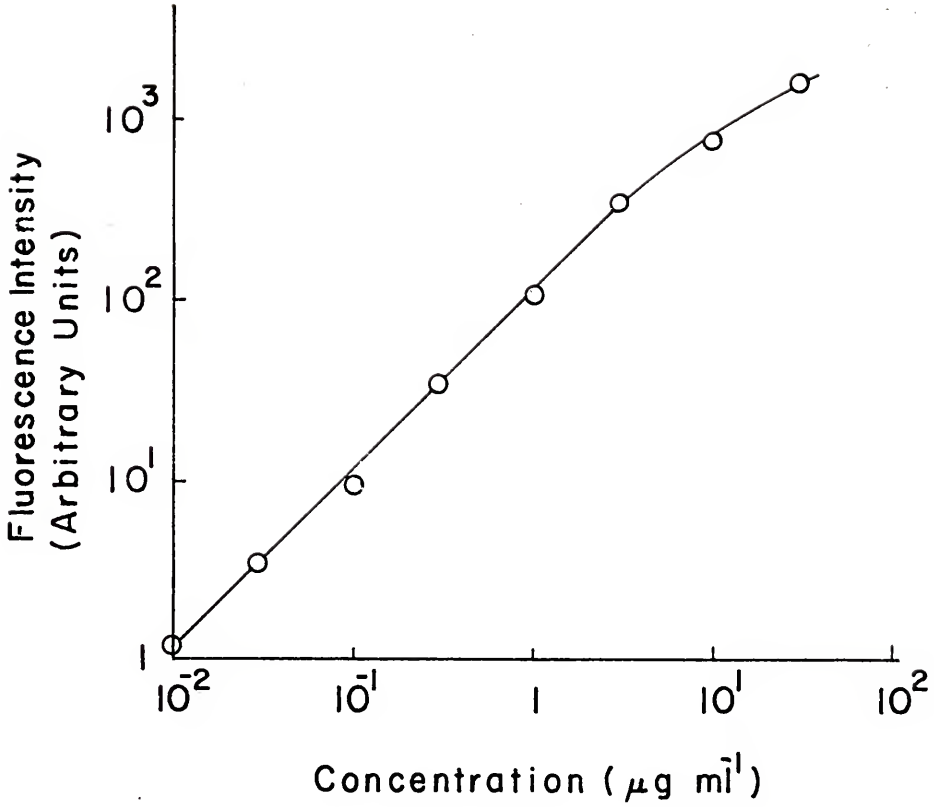

Fig. 16.--Atomic fluorescence analytical curve for Ag in the continuous mode of operation.

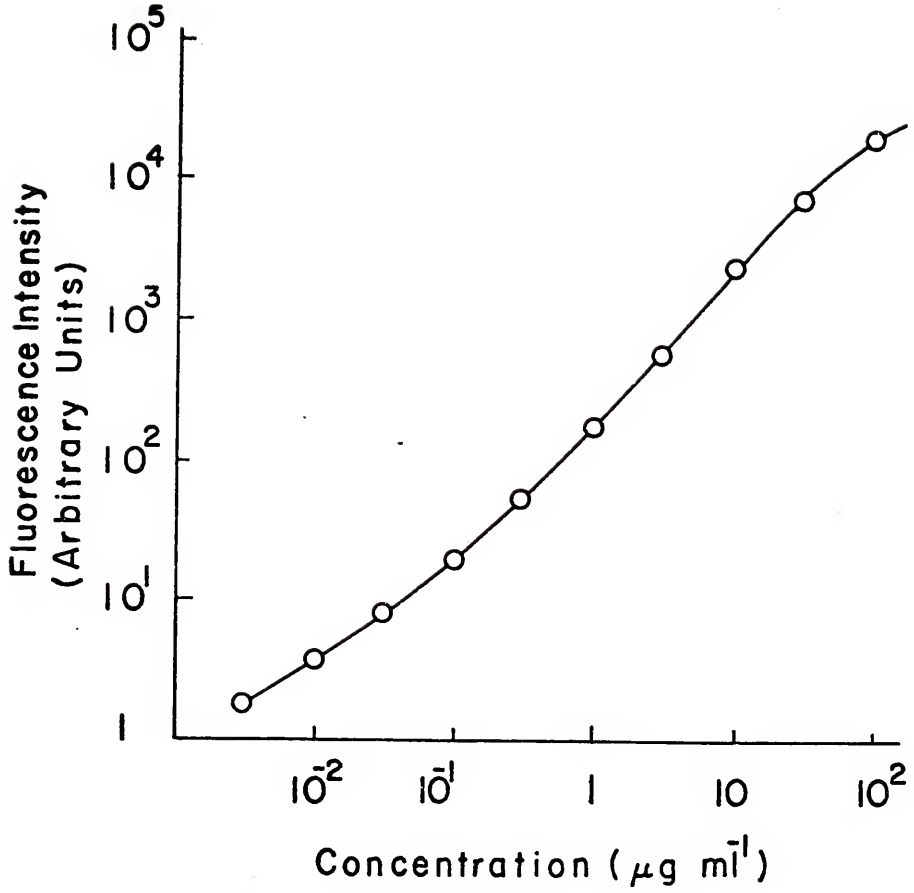

Fig. 17.--Atomic fluorescence analytical curve for Bi in the continuous mode of operation.

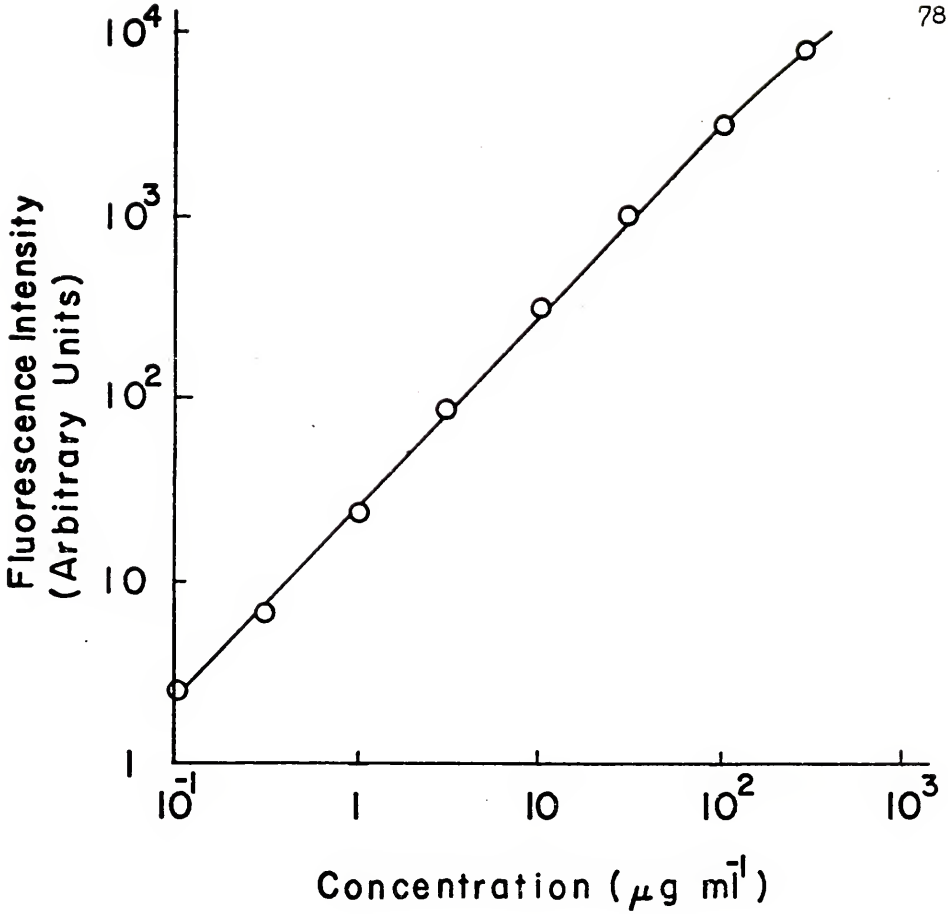

Fig. 18.--Atomic fluorescence analytical curve for Pb in the continuous mode of operation.

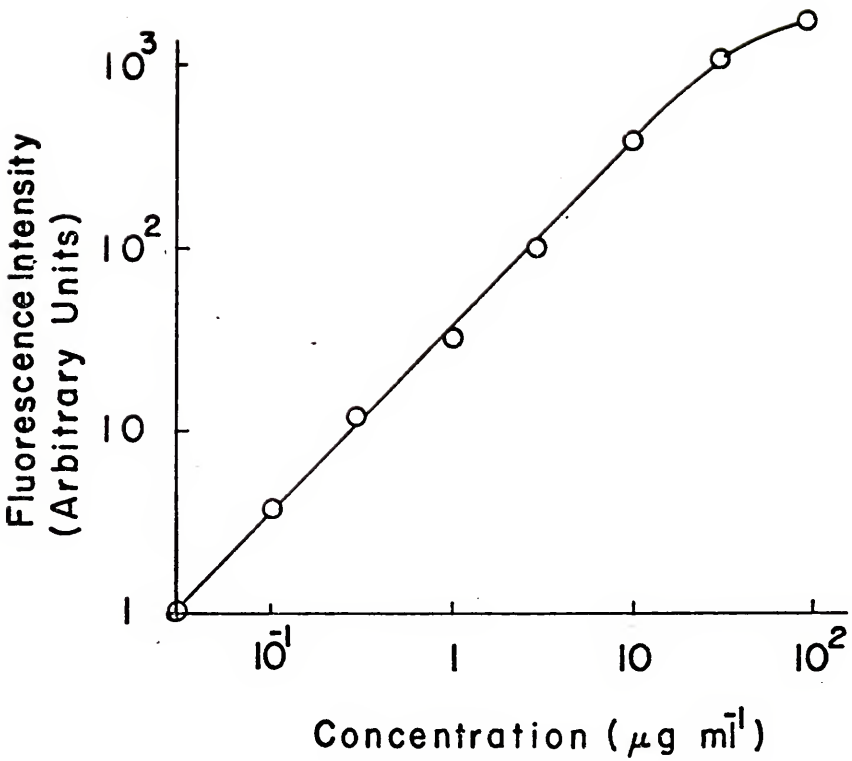

Fig. 19.--Atomic fluorescence analytical curve for Tl in the continuous mode of operation.

Correction for scattering

All atomic fluorescence signals were corrected for any spurious scatter signals by one of two methods, and in all cases the results of the two methods agreed within experimental error. If a source line was available (that is, an Iodine line) which was not a fluorescent line of the analyte, then the ratio of a non-absorbing line intensity, I_{na}, of the source to the primary excitation line, I_F, of the source was calculated.

$$R = \frac{I_{na}}{I_F} \qquad \text{IV-1}$$

Since only lines in the approximate spectral region of fluorescence were used, the variation in photomultiplier spectral response, in spectral transmission of the lenses and all other optical components, was not corrected for. The scatter signal, S_s, and the apparent fluorescence signal, S_F, were then measured, and the corrected scatter signal, S'_{na}, from the atom cell was calculated from

$$S'_{na} = \frac{S}{R} \qquad \text{IV-2}$$

The corrected fluorescence intensity S'_F from the atom cell was then

$$S'_F = S_F - S'_{na} \qquad \text{IV-3}$$

for the first method.

The second procedure used to correct for spurious scatter was

i. measure blank (deionized water) signal, S_b, at the temperature of atomization;

ii. measure apparent fluorescence signal, S_F, for concentration of interest;

iii. decrease the temperature of the vitreous carbon tube furnace to 100 °C and measure any scatter signal, S_s. The maximum scatter signal was then assumed to be S_s and the corrected fluorescence signal S'_f was calculated from

$$S'_F = S_F - S_s - S_b \qquad \text{IV-4}$$

This method assumes that

i. no appreciable atomization has occurred in the vitreous carbon tube furnace in step iii, and hence no atomic fluorescence was measurable;

ii. any scatter signal measured at high temperatures not measured at low temperatures was due to hot carbon particles and radical formation;

iii. the scatter signal due to the analyte could only increase by lowering the temperature of the vitreous carbon tube due to reduced desolvation and possible coagulation.

Since this second method may over-correct for scatter, it was not used in cases where scatter was estimated to be over 4 per cent of the fluorescent signal (see items i and iii listed above).

Precision

The precision for Sn, Pb, Ag, Bi, Tl, and Te is listed in Table 3. The precision obtained is very competitive with all other atomization devices in use for atomic fluorescence. For all elements examined, the relative standard deviation is 0.025 to 0.048, which is comparable to that observed in flame AFS and generally better than that of graphite rod AFS. The present continuous introduction non-flame cell is not subject to the sample placement errors found in the graphite rod atomizers.

Atom population profiles

The method used to measure the decay of atom population-height profiles has been previously described [23,33,34]. Atomic profiles as a function of height above the vitreous carbon tube furnace for several elements were examined in a similar manner for the present atomization cell to determine the effect of only an Ar sheath versus an Ar-H_2 diffusion flame sheath on the decay of atom populations exiting continuously from the present continuous-sampling vitreous carbon tube furnace. The same atomization conditions were used for this study as for the LOD measurements.

The factors contributing to the decrease in the measured peak atomic fluorescence as the vitreous carbon tube furnace was lowered include: (i) the loss of atoms by chemical reaction; (ii) transport of atoms outside the

light path by diffusion; (iii) decrease of the solid angle subtended by the atoms in the sample cavity; (iv) quenching of the excited-state atom populations by collisions, particularly with diatomic and polyatomic species. Even in the absence of condensation, oxide formation, and other possible chemical losses, a gradual decrease of the fluorescence signal from factors (ii) and (iii) would be expected.

The decay of atom populations with height above the vitreous carbon tube furnace for Sn and Pb was measured by atomic fluorescence spectrometry and the results are shown in Figure 20. In the case of Pb with the Ar-H_2 diffusion flame, the decay of the atom populations was gradual, reaching 50 per cent at a height of 20 mm above the furnace exit. With only an Ar sheath, however, the decay of Pb proceeded somewhat faster, reaching 30 per cent of the original population at a height of 20 mm. For Sn, the Ar-H_2 diffusion flame had very great influence on the atom population as a function of height above the furnace tube exit; at 12 mm above the carbon tube, the fluorescence signal actually increased 300 per cent, and then it began to decrease to slightly less than 150 per cent at 24 mm. With only Ar, the Sn population dropped to 28 per cent of the original fluorescence signal at 7 mm.

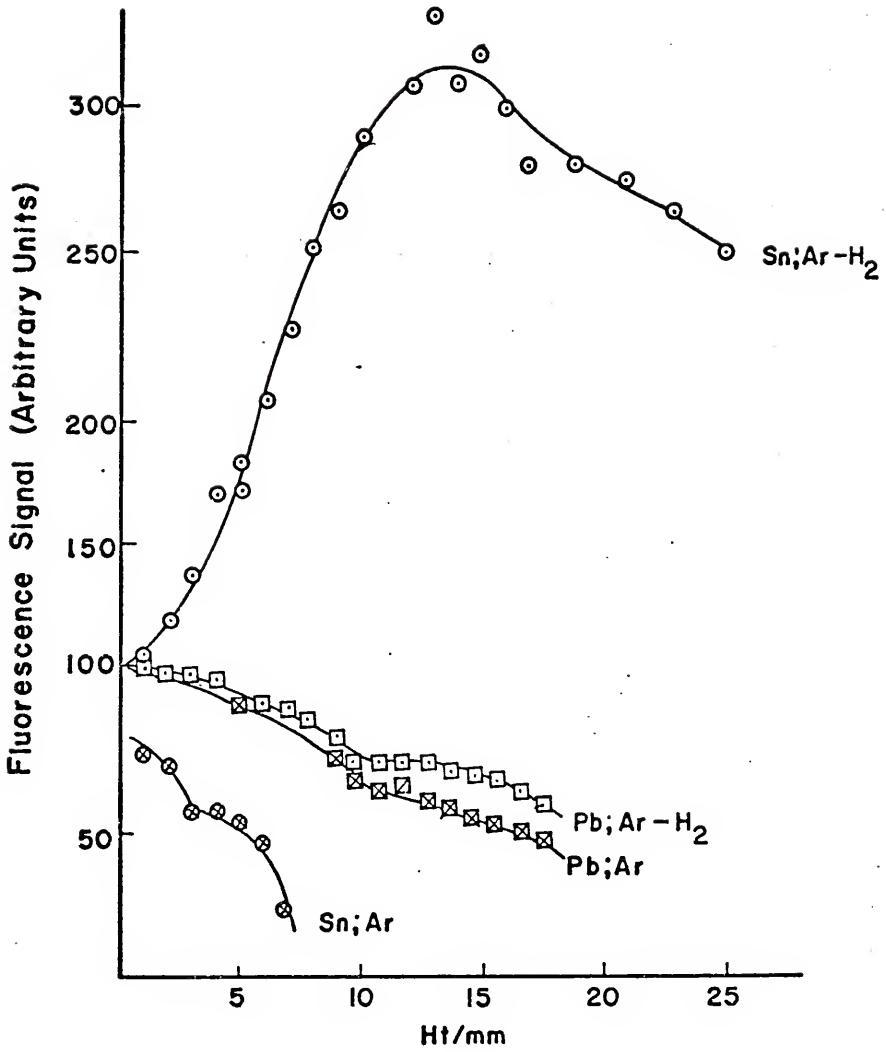

Fig. 20.--Decay of atom populations with height above the vitreous carbon tube atomizer for two elements as measured by atomic fluorescence spectrometry. O, Sn, 3034 Å; □ , Pb, 2833 Å; X, Ar atmosphere; •, Ar/H_2 atmosphere.

For the two elements (Pb and Sn) studied here, the atomic population-height profile was less steep for the present continuous-sample injection non-flame cell compared to that of the discrete graphite carbon filament atomizer [33]. For instance, at a height of 5 mm above the atomizer, the fluorescence signal of Sn with Ar entrainment is about 55 per cent of the initial signal for the present atomizer as compared to less than 2 per cent of the initial signal for the graphite filament atomizer. When a H_2 diffusion flame was used with the present system, the fluorescence signal increased about 3-fold, while with the carbon filament atomizers, fluorescence decreased to about 20 per cent at 15 mm height.

In the case of Pb at 10 mm height above the non-flame cell, the atomic fluorescence signal was about 60 per cent of the initial fluorescence signal with either the Ar or Ar-H_2 entrainment sheath, while in the case of the graphite filament atomizer, the fluorescence signal was less than 30 per cent with a H_2 diffusion flame and less than 1 per cent with only an Ar sheath.

These results tend to indicate that the presence of the H_2 diffusion flame helps to prevent the rapid attenuation of the atomic populations, and in the case of Sn, it actually increases the atomic populations at some heights above the vitreous carbon tube furnace. Previous

studies on a similar type of H_2 diffusion flame suggested that the atomic cell was characterized by a region of an excess unburned H_2, which minimized the entrainment of O_2 [30].

In the case of Sn, where the fluorescence intensity increased to a height of 15 mm over the vitreous carbon tube, the indication was that H_2 was not only protecting the metal atom cloud from oxide formation, but also was assisting in Sn-atom production from the molecules formed previously by reactions such as

$$MO + H_2 \longrightarrow M + H_2O$$

$$MO + H \longrightarrow M + OH$$

where M was some metal. The explanation for why this occurs to a far greater extent with the vitreous carbon tube furnace than with the carbon filament may lie in the higher temperatures of the furnace, which render the H_2 diffusion flame of the former more reactive.

Pulsed-Sampling Mode Results

Limits of detection

The atomic fluorescence limit of detection (LOD) for this study was defined as that concentration (in $\mu g\ ml^{-1}$) giving a fluorescence signal of 3 x rms noise of the blank. The concentration limits of detection, along with the various gas flow rates, temperature of atomization, and EDL

conditions for a 10 ml sample size for each element are given in Table 5. The resulting concentration and absolute LOD's are compared in Table 6 to the best atomic fluorescence limits of detection obtained by previous workers with discrete sampling non-flame cells and flames, as well as to the previous LOD's calculated for the present system used in the continuous-sampling mode. The best concentration and absolute limits of detection obtained by flame atomic absorption, graphite tube atomic absorption, and the plasmas are also given. Generally the concentration limits of detection by the present system operated in the pulsed mode are comparable to most other methods, while the absolute limits of detection by the present non-flame cell were generally superior by 1 order of magnitude or more.

Size of sample

The fluorescence signal did not increase linearly with increasing sample sizes of 1 µl, 5 µl, and 10 µl for the three elements shown in Figure 21. The figure indicates that the best atomization efficiency is obtained for 1 µl and 5 µl samples, while the efficiency drops off slightly for the 10 µl sample size.

TABLE 5

EXPERIMENTAL CONDITIONS AND ANALYTICAL RESULTS FOR MEASUREMENT OF SEVERAL ELEMENTS BY MEANS OF THE PULSED-SAMPLE INTRODUCTION TUBE FURNACE ATOMIC FLUORESCENCE SPECTROMETRIC SYSTEM

Element	Wavelength (nm)	EDL Conditions		Tube Furnace Conditions					LOD[f] ($\mu g\ ml^{-1}$)	RSD[g]	V[h] (μl)
		Temp.[a] (°C)	Power[b] (W)	Temp.[c] (°C)	Ar Flow Rate Nebulizer ($l\ min^{-1}$)	Ar Flow Rate[d] External ($l\ min^{-1}$)	H_2 Flow Rate[d] External ($l\ min^{-1}$)	CH_4 Flow Rate[e] Internal ($l\ min^{-1}$)			
Ag	328.1	540	50	1580	0.66	5.3	0.0	0.014	4×10^{-4}	0.028	10
Te	213.9	440	30	1550	0.66	5.3	2.2	0.014	3×10^{-3}	0.036	10
Sn	303.4	285	90	1720	0.66	5.3	2.2	0.014	2×10^{-2}	0.021	10
Tl	377.6	385	50	1540	0.66	5.3	2.2	0.014	2×10^{-3}	0.031	10
Bi	307.7	510	50	1540	0.66	5.3	2.2	0.014	6×10^{-4}	0.036	10
Pb	283.3	430	40	1580	0.66	5.3	2.2	0.014	5×10^{-3}	0.033	10
Co	240.7	200	100	1860	0.66	5.3	0.0	0.014	3×10^{-3}	0.031	10
Sb	231.1	125	100	1650	0.66	5.3	2.2	0.014	1×10^{-2}	0.035	10
Cd	228.8	360	70	1540	0.66	5.3	2.2	0.014	4×10^{-5}	0.022	10

Table 5 Continued

Element	Wavelength (nm)	EDL Conditions		Tube Furnace Conditions					LOD[f] ($\mu g\ ml^{-1}$)	RSD[g]	$V_{(\mu l)}$[h]
		Temp.[a] (°C)	Power[b] (W)	Temp.[c] (°C)	Ar Flow Rate Nebulizer ($l\ min^{-1}$)	Ar Flow Rate[d] External ($l\ min^{-1}$)	H_2 Flow Rate[d] External ($l\ min^{-1}$)	CH_4 Flow Rate[e] Internal ($l\ min^{-1}$)			
Zn	213.8	480	30	1540	0.66	5.3	2.2	0.014	$2x10^{-4}$	0.026	10
Mg	285.2	410	100	1940	0.66	5.3	2.2	0.014	$5x10^{-2}$	0.036	10

[a] Temperature of air flowing by EDL.

[b] Microwave power applied to EDL using thermostated "A" antenna.

[c] Temperature of graphite tube furnace walls.

[d] Flow rate of Ar and/or H_2 around tube furnace exit.

[e] Flow rate of CH_4 through tube furnace.

[f] LOD = limit of detection (see text for definition).

[g] RSD = relative standard deviation (taken at a concentration of about 100xLOD).

[h] $V_{(\mu l)}$ = volume size of discrete sample.

Table 6

COMPARISON OF FLAME AND NON-FLAME ATOMIZATION ATOMIC ABSORPTION AND FLUORESCENCE LIMITS OF DETECTION AND PLASMA TORCH LIMITS OF DETECTION

Element	TUBE NON-FLAME CELL (This Study) Continuous LOD		TUBE NON-FLAME CELL (This Study) Pulsed LOD		ATOMIC FLUORESCENCE FLAME LOD		Ref.	ATOMIC FLUOURESCENCE FILAMENT NON-FLAME CELL LOD		Ref.	ATOMIC ABSORPTION FLAME LOD		Ref.	ATOMIC ABSORPTION TUBE NON-FLAME CELL LOD		Ref.	ATOMIC EMISSION PLASMA TORCH LOD		Ref.
	Conc. ($\mu g\ ml^{-1}$)	Abs. (ng)	Conc. ($\mu g\ ml^{-1}$)	Abs. (ng)	Conc. ($\mu g\ ml^{-1}$)	Abs. (ng)		Conc. ($\mu g\ ml^{-1}$)	Abs. (ng)		Conc. ($\mu g\ ml^{-1}$)	Abs. (ng)		Conc. ($\mu g\ ml^{-1}$)	Abe. (ng)		Conc. ($\mu g\ ml^{-1}$)	Abs. (ng)	
Ag	$2x10^{-4}$	$2x10^{-2}$	$4x10^{-4}$	$4x10^{-3}$	$1x10^{-4}$	$5x10^{-1}$	86	$8x10^{-4}$	$4x10^{-4}$	33	$2x10^{-3}$	$2x10^{-1}$	91	$2x10^{-6}$	$2x10^{-4}$	91	$2x10^{-2}$	$1x10^{1}$	92
Te	$2x10^{-3}$	$1x10^{-1}$	$3x10^{-3}$	$3x10^{-2}$	$6x10^{-3}$	$3x10^{1}$	85	-	-	-	-	-	-	-	-	-	$2x10^{-1}$	$1x10^{2}$	92
Tl	$6x10^{-5}$	$7x10^{-1}$	$2x10^{-3}$	$2x10^{-2}$	$8x10^{-3}$	$4x10^{1}$	86	$4x10^{-2}$	$2x10^{-2}$	33	$1x10^{-4}$	$1x10^{-2}$	91	$1x10^{-4}$	$1x10^{-2}$	91	$2x10^{-1}$	$1x10^{2}$	92
Bi	$2x10^{-3}$	$2x10^{-1}$	$6x10^{-4}$	$6x10^{-3}$	$5x10^{-3}$	$2x10^{1}$	85	$1x10^{-2}$	$1x10^{-2}$	17	$1x10^{-4}$	$1x10^{-2}$	91	$1x10^{-4}$	$1x10^{-2}$	91	$5x10^{-2}$	$3x10^{1}$	92
Pb	$1x10^{-2}$	$1x10^{0}$	$5x10^{-3}$	$5x10^{-2}$	$1x10^{-2}$	$5x10^{1}$	84	$5x10^{-3}$	$3x10^{-3}$	36	$6x10^{-5}$	$6x10^{-3}$	91	$6x10^{-5}$	$6x10^{-3}$	91	$2x10^{-3}$	$2x10^{-1}$	93
Sn	$1x10^{-2}$	$1x10^{0}$	$1x10^{-2}$	$1x10^{-1}$	$1x10^{-1}$	$5x10^{2}$	83	$2x10^{-1}$	$1x10^{-1}$	33	$1x10^{-2}$	$1x10^{0}$	91	-	-	-	$3x10^{-2}$	$3x10^{0}$	93
Sb	-	-	$1x10^{-2}$	$1x10^{-1}$	$5x10^{-2}$	$2x10^{2}$	88	$7x10^{-1}$	$2x10^{-1}$	9	$2x10^{-4}$	$2x10^{-2}$	91	$2x10^{-4}$	$2x10^{-2}$	91	$2x10^{-1}$	$1x10^{2}$	92
Mg	-	-	$5x10^{-2}$	$5x10^{-1}$	$1x10^{-4}$	$7x10^{-1}$	89	$1x10^{-3}$	$1x10^{-3}$	17	-	-	-	-	-	-	$2x10^{-4}$	$2x10^{-2}$	93
Cd	-	-	$4x10^{-5}$	$4x10^{-4}$	$1x10^{-6}$	$5x10^{-3}$	86	$3x10^{-5}$	$3x10^{-5}$	36	$1x10^{-6}$	$1x10^{-4}$	91	$1x10^{-6}$	$1x10^{-4}$	91	$3x10^{-3}$	$3x10^{-1}$	93
Zn	-	-	$2x10^{-4}$	$2x10^{-3}$	$4x10^{-5}$	$2x10^{-1}$	87	$2x10^{-5}$	$2x10^{-5}$	17	$6x10^{-7}$	$6x10^{-5}$	91	$6x10^{-7}$	$6x10^{-5}$	91	$9x10^{-3}$	$5x10^{0}$	92
Co	-	-	$3x10^{-3}$	$3x10^{-2}$	$5x10^{-3}$	$2x10^{1}$	90	$2x10^{-2}$	$2x10^{-2}$	23	$4x10^{-5}$	$4x10^{-3}$	91	$4x10^{-5}$	$4x10^{-5}$	91	$3x10^{-3}$	$2x10^{0}$	92

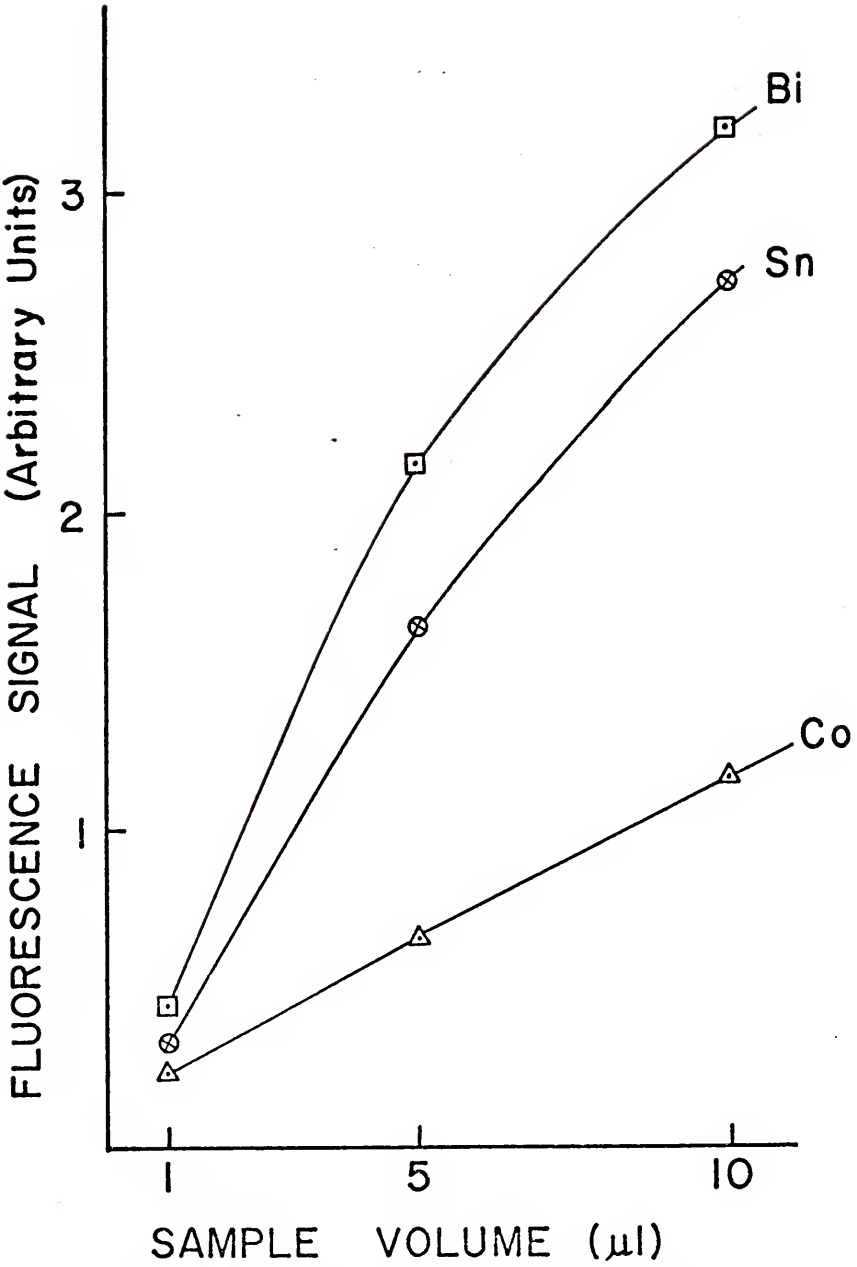

Fig. 21.--Fluorescence signal versus sample size for Bi, Sn, and Co with pulsed mode of operation.

Linear dynamic range and sensitivity

The pulsed mode linear dynamic ranges for three elements (Sn, Bi, and Co) are shown in Figures 22, 23, and 24. Both Sn and Bi were found to have the same linear dynamic ranges in the pulsed mode as in the continuous mode of operation ($2x10^3$ and $1x10^4$, respectively) after accounting for differences in source intensity. The linear dynamic range for Co was even greater, that is, $3x10^4$. The sensitivities of Sn, Bi, and Co were found to be 0.88, 0.90, and 0.61, respectively.

Precision

The relative standard deviation (RSD) for the eleven elements measured by atomic fluorescence spectrometry using pulsed mode atomization for concentrations at approximately 100 - 200 x LOD is listed in Table 5. For the eleven elements determined, the precision was found to be between 0.021 and 0.036 with an average value of about 0.030. These values are slightly better than found for the continuous mode and for the flame, as well as most other non-flame atomizers in atomic fluorescence spectrometry.

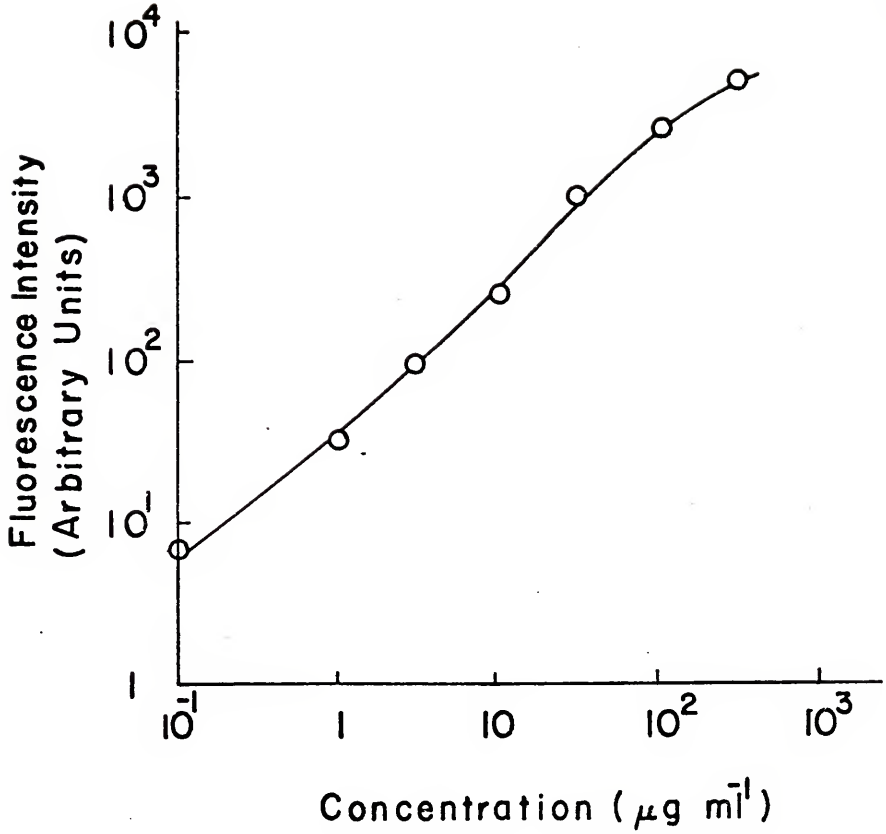

Fig. 22.--Atomic fluorescence analytical curve for Sn in the pulsed mode of operation.

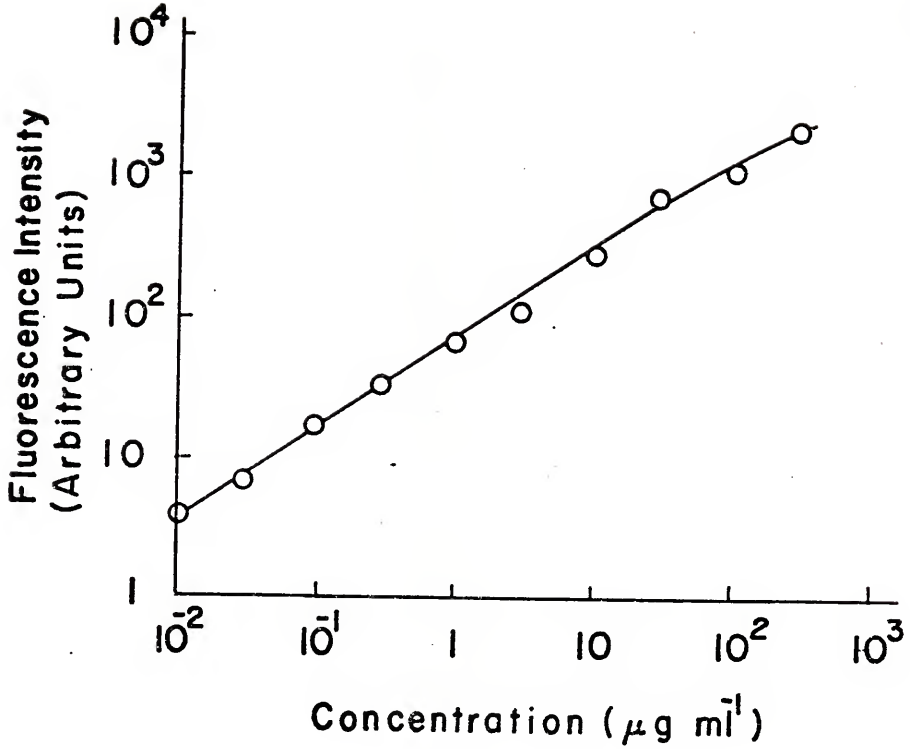

Fig. 23.--Atomic fluorescence analytical curve for Co in the pulsed mode of operation.

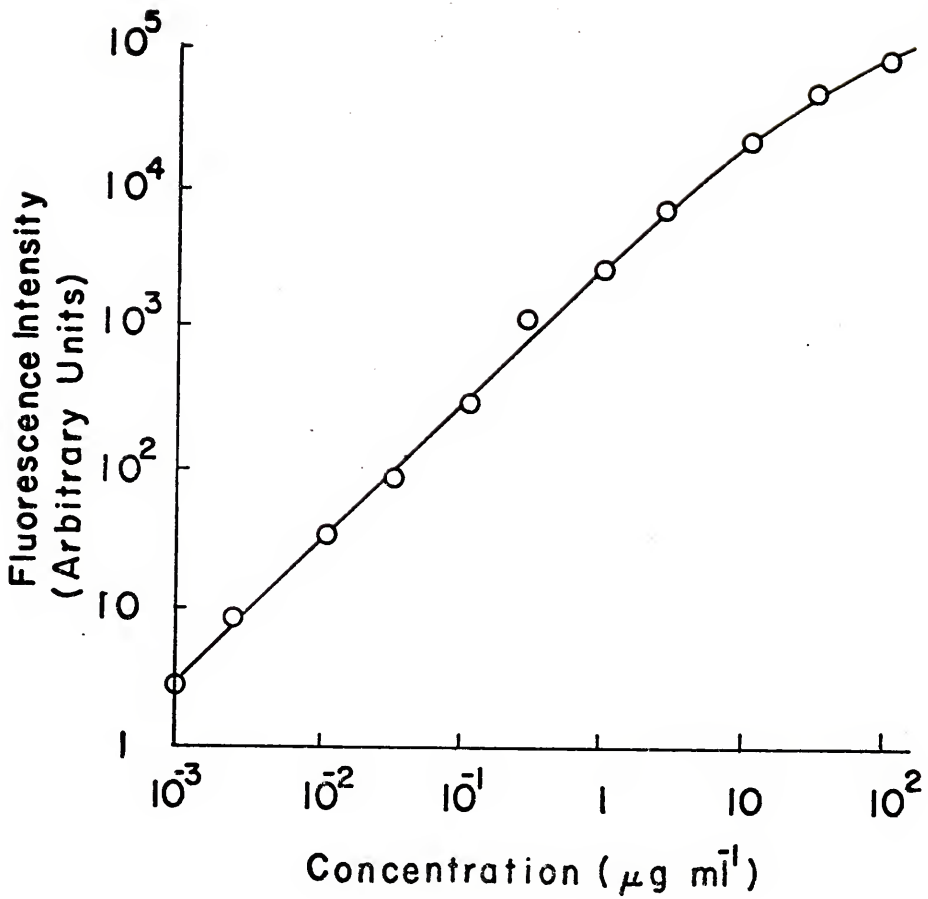

Fig. 24.--Atomic fluorescence analytical curve for Bi in the pulsed mode of operation.

CHAPTER V

SUMMARY AND FUTURE WORK

Summary

Resistively heated non-flame cells previously used for atomic absorption and atomic fluorescence spectroscopy have been reviewed. A versatile new type of resistively heated non-flame cell usable in both the continuous introduction and the pulsed introduction modes has been described, and analytical figures of merit in atomic fluorescence spectrometry have been given.

The theory of the conversion of the analyte to an atomic fluorescence signal was reviewed, along with some reasons why non-flame cells in atomic fluorescence spectrometry should attain better signal-to-noise ratios than flame atomic fluorescence spectrometry. The theories of transient and continuous signals were discussed, and methods to obtain maximum signal-to-noise ratios for each have been described.

The design, construction, and evaluation of the new versatile resistively heated non-flame cell were discussed. The non-flame cell system consisted of a very efficient

pneumatic nebulizer operated at high pressures with low sample consumption for introduction of a fine sample aerosol into a vitreous carbon tube furnace via a desolvation chamber. Atomic vapor of several metals (Sn, Pb, Te, Ag, Tl, and Bi) was produced by continuous pneumatic nebulization of an aqueous sample through a vitreous carbon tube furnace, and atomic fluorescence was excited with single-element electrodeless discharge lamps. The high efficiency of the system has been considered along with precision, sensitivity, linear dynamic range, and limits of detection for the elements examined. The decay of atom populations above the furnace outlet using either an Ar-H_2 diffusion flame sheath or an Ar sheath was determined, and the results have been discussed.

Pulsed pneumatic nebulization of aqueous samples, containing various metals (Ag, Bi, Cd, Co, Mg, Pb, Sb, Sn, Te, Tl, and Zn), into a vitreous carbon tube furnace produced metal vapors which were excited with single-element electrodeless discharge tube lamps, and the resulting atomic fluorescence was measured. This mode of operation improved the absolute limits of detection; no deleterious effects to the linear dynamic ranges resulted. The long lifetime of the vitreous carbon tube was also discussed. The atomic fluorescence intensity versus different sample sizes for a few elements has been considered.

Additional advantages of the present non-flame cell system over some past non-flame cells are that operator error due to sample placement is eliminated, and that the conversion of the atomizer from the continuous mode to the pulsed mode of sampling was achieved by simply altering the means of sample injection.

Future Work

Desolvation chamber considerations

In Figure 25, the peak shape obtained when measuring the atomic fluorescence intensity versus time is shown for a concentration of 30 $\mu g\ ml^{-1}$ of Sn at 303.4 nm. The signal is seen to decrease in an exponential fashion with time; however, it does not rigorously obey Equation II-25 for an exponential dilution flask.

$$n_t = n_o e^{-(ut/V)} \qquad \text{II-25}$$

This equation may be rearranged by taking logarithms of both sides to give

$$2.3 \log n_t = 2.3 \log n_o - (U/V)t \qquad \text{V-1}$$

In the plot of $2.3 \log n_t$ versus t, -(U/V) is the slope and the intercept is $2.3 \log n_o$. Equation II-25 is valid if a completely homogeneous concentration of analyte resulted throughout the desolvation chamber before any analyte exited. Of course, to obtain the maximum atomic

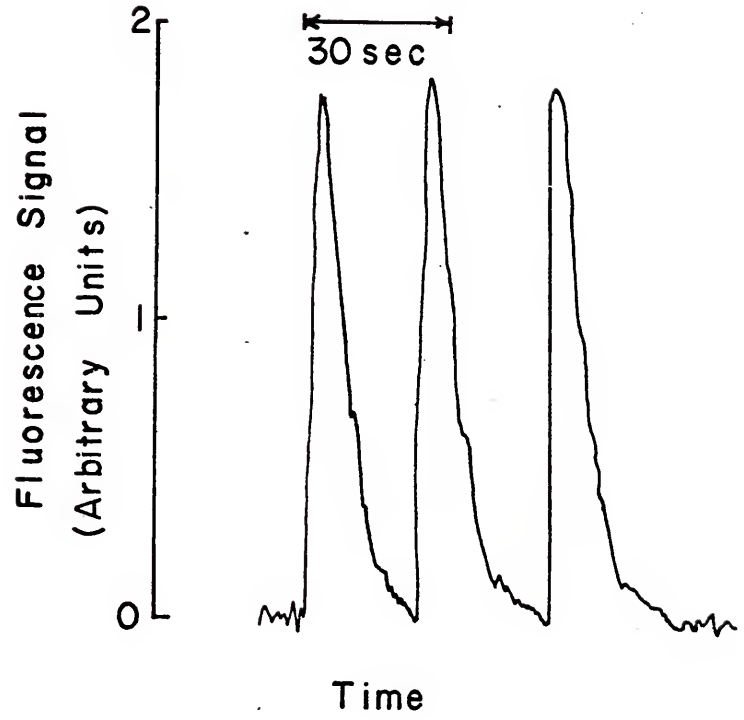

Fig. 25.--Fluorescence signal versus time after introduction of three pulsed samples of 10 µl of 30 µg ml^{-1} Sn at 303.4 nm.

fluorescence signal, dilution of the analyte atoms must be minimized.

Using the above-mentioned theory, a modified stainless steel desolvation chamber was constructed, shown in Figure 26. So as not to affect the transport efficiency, the volume of the desolvation chamber was kept large enough to allow the aerosol to undergo a multiple number of desolvation times, t_d, for the estimated chamber size. The volume of the modified desolvation chamber was chosen to be 8 cm^3 allowing a time of desolvation of about 15 t_d before any constrictions occurred in the desolvation chamber and greater than 30 t_d in total residence time in the desolvation chamber (when an Ar nebulization flow rate of 0.66 1 min^{-1} was used). The shape of the modified desolvation chamber was chosen to reduce the dilution of the analyte pulse in the desolvation chamber due to turbulence and to still allow rather straightforward machining.

Figure 27 shows theoretical plots (from Equation V-1) for the logarithm of the concentration versus time for the two desolvation chamber volumes utilized in this dissertation (80 cm^3 and 8 cm^3), where exponential dilution behavior was assumed. From the exponential dilution theory, one would predict a gain in signal at t = 0 of 1 order of magnitude; however, the limit of detection for Sb by atomic fluorescence spectrometry decreased by more than a factor

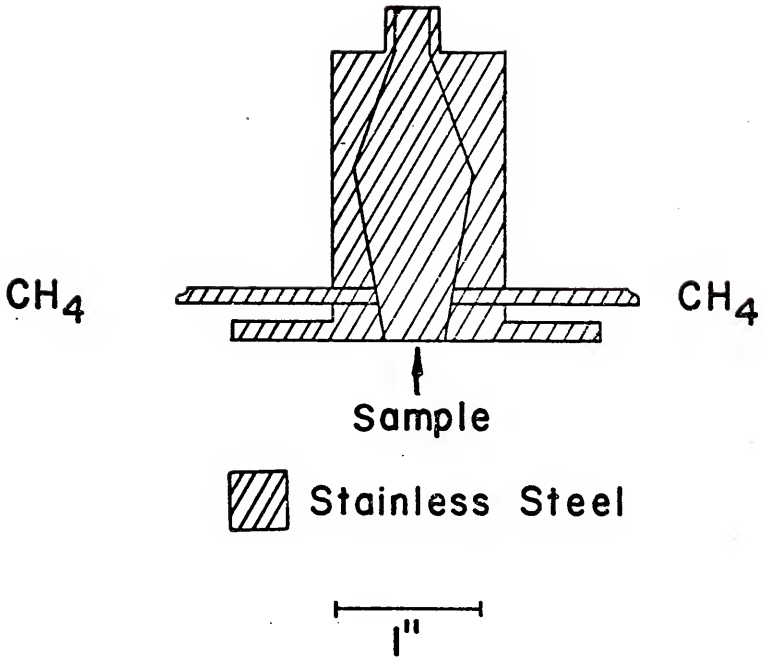

Fig. 26.--Schematic diagram of a modified stainless steel desolvation chamber.

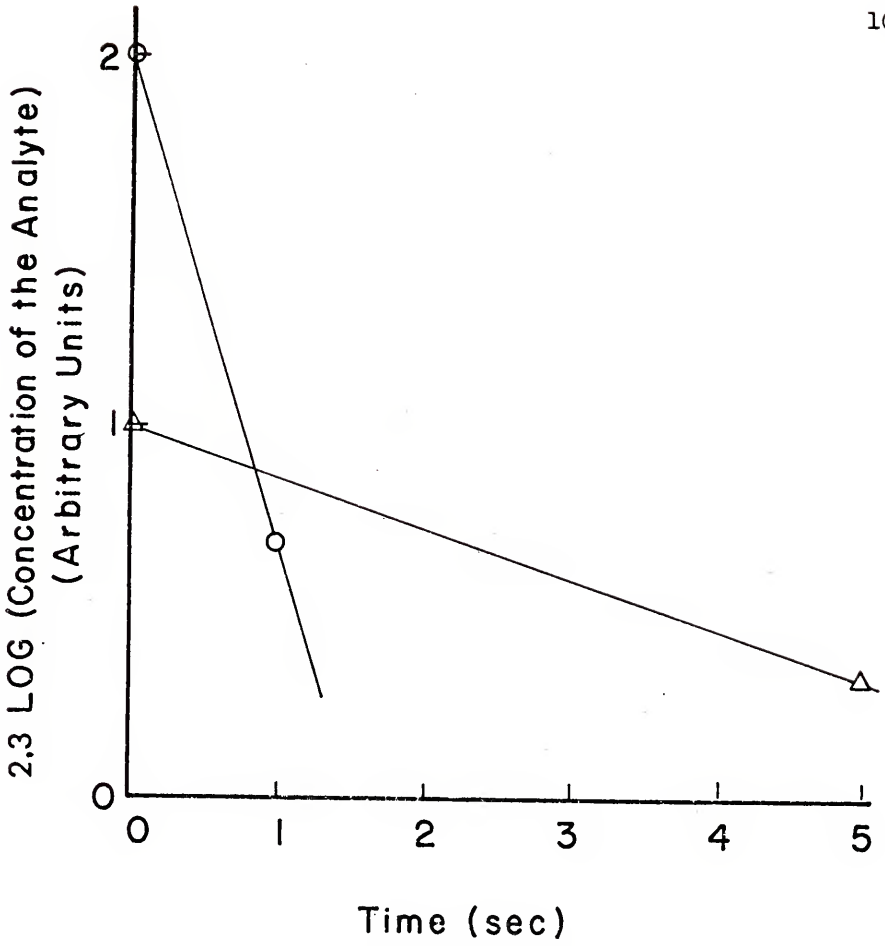

Fig. 27.--2.3 Log concentration in the atom cell versus time after introduction of the pulsed sample for two volumes of exponential dilution flasks with identical initial amounts of analyte.

O = 8 ml desolvation chamber
Δ = 80 ml desolvation chamber.

of 20 when the desolvation chamber volume was decreased by this order of magnitude. This deviation from exponential dilution theory may result because neither desolvation chamber contains a homogeneous aerosol at t = 0. However, the aerosol in the 80 cm^3 chamber is probably more homogeneous.

Atomic emission considerations

The atomic emission intensity of atoms excited in a non-flame atomic cell in which the species are in thermal equilibrium may be approximated with the Boltzmann equation (Equation II-28) already discussed. From this equation, it is evident that the emission intensity depends heavily upon the temperature of the atom cell; an increase in temperature leads to an increase in atomic emission intensity.

Because the atom cell attains a lower "temperature" (not known whether it is a thermodynamic temperature) than most flames (see Figure 13) which attain temperatures of 2000-2800 degrees, the possibility of thermal excitation-emission is low. It is a well-known fact, however, that emission may occur due to other reasons such as chemiluminescence [94-96].

A few elements were examined to predict the future usefulness of non-flame cell atomic emission, and the results appear very encouraging. Elements of Sr, Cd, and K resulted in limits of detection in the $\mu g\ ml^{-1}$ range or

lower at wavelengths of 404.4 nm, 326.1 nm, and (766.5 nm and 404.4 nm), respectively, when the various gas flow rates and temperatures were optimized. The flow rates of some of the respective gases, especially the external H_2, were very critical, as was the gas temperature. In all cases, higher gas temperatures led to lower emission detection limits.

Of the three elements, Sr, Cd, and K, K at a wavelength of 766.5 nm was evaluated the most completely. In Figure 28, a plot of intensity versus the temperature of a restricted area of viewing is shown where spatial "thermal equilibrium" was approximated. The lower limit of detection of K was approximately 5×10^{-5} $\mu g\ ml^{-1}$ with a linear dynamic range of about 2 orders of magnitude for a pulse size of 5 μl.

When measuring the intensity of emission from 1×10^{-3} $\mu g\ ml^{-1}$ KCl in deionized water, the external Ar flow rate had little effect, and a flow rate of 4.5 l min^{-1} of Ar was used to examine the effect of external H_2. A plot of emission intensity versus the H_2 flow rate is given in Figure 29. The emission was measured from a rectangular area 2 mm high and 8 mm wide at grazing incidence, so that spatial "thermal equilibrium" was approximated. Temperature measurements with tungsten-tungsten 26 per cent rhenium thermocouples were repeated over the range of H_2 flow rates used, and the temperature remained stable at 1240 + 20 °C.

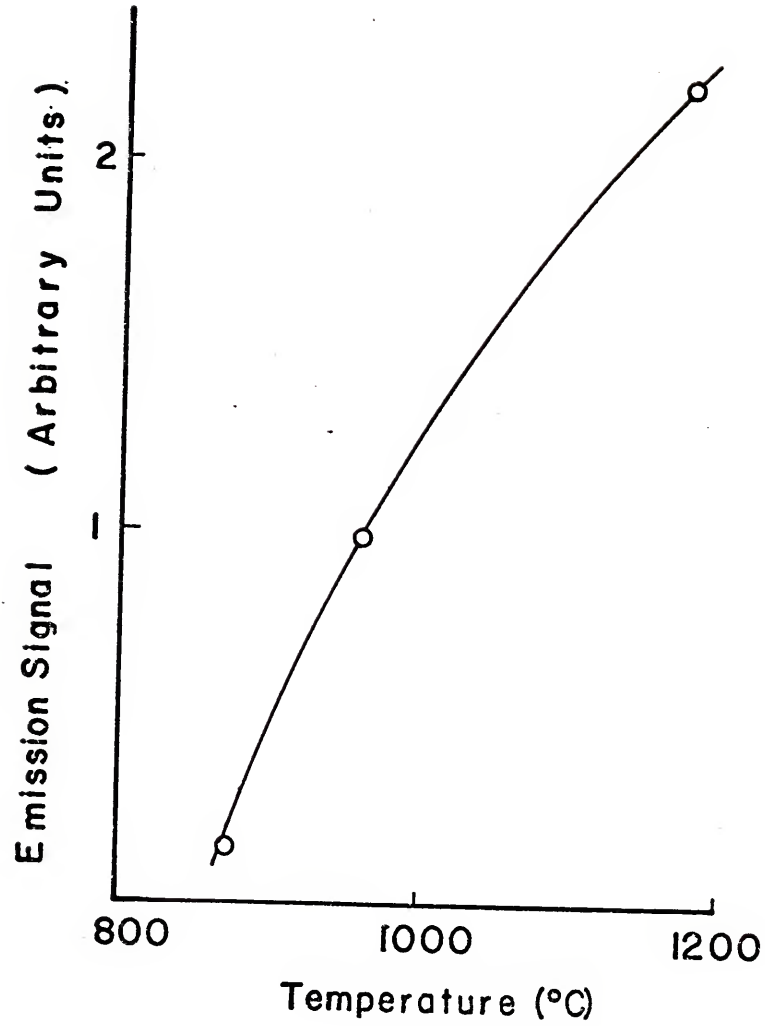

Fig. 28.--Emission signal versus gas temperature at grazing incidence to the vitreous carbon tube.

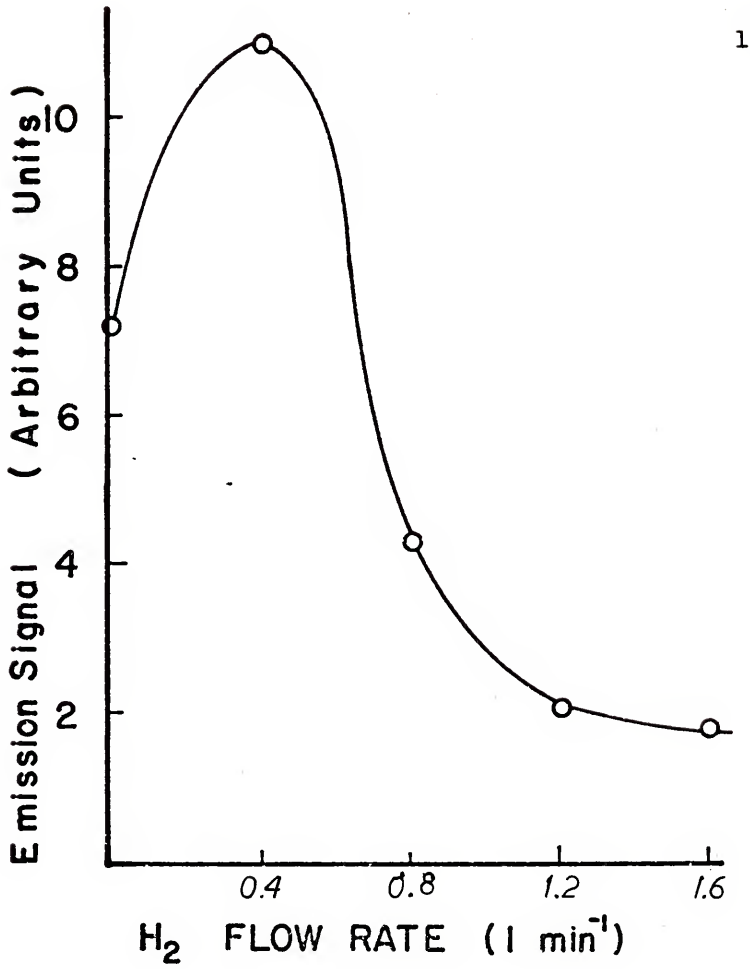

Fig. 29.--Emission signal versus external H_2 flow rate.

The change in K emission intensity, due to change in H_2 flow rate, is much greater than that predicted by the Boltzmann equation for a change of 40 °C.

A solution containing 10 μg ml^{-1} of $NaNO_3$ with 10^{-3} μg ml^{-1} of KCl had no effect upon the emission intensity. The same concentration of KCl in 10 per cent concentrated HCl depressed the emission intensity to 11 per cent of that found with KCl diluted with deionized water.

All emission measurements were performed with a monochromator slit width of 1 mm and emission intensity was amplified with a custom-built DC nanoamplifier [97]. No mirrors were used to increase the solid angle of atomic emission collected by the monochromator; all other experimental conditions and components were identical to those used in the atomic fluorescence measurements previously described (except for omission of the EDL source and associated optics).

Atomic absorption considerations

Atomic absorption with this type of vitreous carbon tube non-flame cell should be investigated, although it is a well-known fact that longer absorption path lengths in the atom cell are desirable to attain lower limits of detection. The effective path length could be straightforwardly increased by mounting a second vitreous carbon tube at grazing incidence to the vitreous carbon furnace

and parallel to the source radiation. This would increase the path length, and consequently the number of atoms in the absorption path length. In the pulsed mode of operation, this would have the further advantage of increasing the residence time of the atoms in the atom cell if a judicious choice of the second tube size is made.

Stop-flow considerations

A very interesting study of the effects of residency time in the vitreous carbon tube at different temperatures for different elements would be an obvious advantage in studying atomization efficiency. This could be achieved quite readily by stop-flowing the system, as Kahn and Slavin [15] did with L'vov's system. The present system could also be enclosed and a reverse pressure pulse of Ar could achieve the same effect. A more direct means of observing the effect of residency times on atomization efficiencies may be achieved by the use of an ultrasonic nebulizer, because the efficiency of aspiration-solute vaporization is not as sensitive to gaseous flow rates in ultrasonic nebulizers as it is in pneumatic nebulizers.

Conventional resistively heated non-flame cell

By placing a receptacle in the bottom of the vitreous carbon tube furnace suitable to receive liquid samples directly from a microliter syringe, the furnace may be

operated with all advantages of a filament non-flame cell, but will have increased residency times and increased potential temperatures due to the excellent baffling of the black-body continuum emitted from the vitreous carbon tube. With this method of operation, dry, ash, and atomize cycles could obviously be used. The carbon tube could also be replenished by the method previously discussed.

APPENDICES

APPENDIX I

DEFINITION OF SYMBOLS

B_F = fluorescence radiance (erg sec^{-1} cm^{-2} sr^{-1})

E_A = total irradiance per unit area absorbed by the spectral line which results in fluorescence (erg sec^{-1} cm^{-2})

A_s = total atom cell surface area (cm^2)

Y' = quantum efficiency (dimensionless)

L = fluorescence path length (cm)

l' = atom cell height (cm)

Ω_A = solid angle over which excitation occurs (sr)

B_{S_i} = incident spectral radiance of the exciting radiation at line i (erg sec^{-1} cm^{-2} sr^{-1})

K_{T_i} = total absorption factor for absorbing line i (sec^{-1})

K_T and B_S = values evaluated at resonance frequency

K_{lu} = modified atomic absorption coefficient for pure Doppler broadening (cm^2)

n_o = concentration of atoms in the ground state (cm^{-3})

X_l = fraction of analyte atoms in the lower state involved in the absorption transition $l \longrightarrow u$, where l is the lower state and u is the upper state (dimensionless)

f_{lu} = absorption oscillator strength transition $l \longrightarrow u$ (dimensionless)

δ_{lu} = factor to account for finite half-width of the line source compared to the absorption line (dimensionless)

l = absorption path length (cm)

a_F = damping constant for atomic fluorescence (dimensionless)

K_F = modified absorption coefficient for reabsorption of fluorescence (cm^2)

X_F = fraction of atoms in lower state involved in reabsorption of fluorescence (dimensionless)

F_F = absorption oscillator strength for reabsorption of fluorescence (dimensionless)

$C_1 = \sqrt{\pi}/2\ \ln\sqrt{2}$ (dimensionless)

$\Delta\lambda_D$ = Doppler half-width of the absorption line (nm)

λ_{lu} = absorption line peak for transition $l \longrightarrow u$ (cm)

$B_{C\lambda_{lu}}$ = spectral radiance for a continuum source (erg sec^{-1} cm^{-2} sr^{-1} nm^{-1})

$C_2 = \sqrt{\pi}/\ln 2$ (dimensionless)

Q = ratio of the quantum efficiency of the analyte in a non-flame cell to the quantum efficiency of the analyte in a flame cell (dimensionless)

Y'_{n-f} = quantum efficiency of the analyte in a non-flame cell (dimensionless)

Y'_f = quantum efficiency of the analyte in a flame cell (dimensionless)

k_f = 1st order rate constant for radiational deactivation of the resonance level (sec^{-1})

k_{Q_i} = 2nd order quenching rate constant for deactivation of the resonance level by collisions of element with a quencher Q_i (cm^3 sec^{-1})

n_{Q_i} = concentration of quencher (cm^{-3})

Δi_{tot} = total noise (V, A, or arbitrary units)

Δi_1, Δi_2 = individual sources of random noise (V, A, or arbitrary units)

N_o = number of analyte atoms consumed (dimensionaless)

N = total number of atoms of the analyte in the atom cell at time, t (dimensionless)

τ_1 = duration of transfer of atoms into the atom cell (sec)

τ_2 = average residency time of the analyte in the cell (sec)

τ_3 = time the signal is recorded for (sec)

$n_1(t)$ = number of atoms entering the cell at time, t (dimensionless)

$n_2(t)$ = number of atoms escaping from the cell at time, t (dimensionless)

W/V = ratio of the flow rate of aspiration gas (l sec^{-1}) to volume of aspiration cell (l)

N(t)= original electronic peak shape

i(t)= distorted electronic peak shape

A(t)= transient characteristic of the electronic circuit

τ_c = length of time during which the output signal is within 36.8 per cent of input signal (sec)

R = resistance (ohms)

C = capacitance (Farads)

U = flow rate of aspirating gas (cm^3 sec^{-1})

n_t = concentration of atoms at time (t) in atom cell (cm^{-3})

n_o = initial concentration at time t = 0 of analyte in atom cell (cm^{-3})

v = volume of sample solution pulse (cm^3)

V = volume of exponential dilution flask (cm^3)

c = concentration of analyte in sample solution prior to aspiration (mol cm^{-3})

N_A = Avogadro's number (mol $^{-1}$)

ϵ = efficiency of aspiration (dimensionless)

β = free atom fraction (dimensionless)

e_f = gas expansion factor (dimensionless)

Z_t = ratio of atoms in the ground state to total number in all states (dimensionless)

F = sample flow rate (cm^3 min^{-1})

Q = flow rate of gas entering cell (cm^3 sec^{-1})

n_o = number of atoms in the ground state (dimensionless)

n_s = number of atoms in a level with an excitation energy of E_s (dimensionless)

gs,go = weighting factors (dimensionless)

k = Boltzmann's constant (8.614×10^{-5} eV $^oK^{-1}$)

T = atom cell temperature (°K)

E_s = excitation energy of level s (eV)

$_T$ = total atom population (dimensionless)

$\underline{C}$ = limit of detection (mol l^{-1})

m = slope of the analytical curve (dimensionless)

$\underline{S}$ = smallest measurable signal (V, A, or arbitrary units)

$\bar{S}_{s+b}$ = average limiting signal due to analyte plus blank (V, A, or arbitrary units)

$\bar{S}_b$ = average blank signal (V, A, or arbitrary units)

σ_s = standard deviation of the signal (V, A, or arbitrary units)

σ_{s+b} = standard deviation of the signal plus blank (V, A, or arbitrary units)

n_b = number of measurements performed on the blank signal (dimensionless)

n_s = number of measurements performed on the analyte signal (dimensionless)

Z = Z-statistic of the normal distribution (dimensionless)

t = student t (dimensionless)

s_s = estimated standard deviation (V, A, or arbitrary units)

s_b = estimated standard deviation of the signal (V, A, or arbitrary units)

d = mean particle diameter (µm)

ν = velocity aspiration gas (m sec^{-1})

σ = surface tension (dyn cm^{-1})

ρ = density of liquid (g ml^{-1})

V_L = volume of the liquid (l)

V_a = volume of aspiration gas (l)

η = viscosity (dyn sec^{-1} cm^{-2})

ρ = density of liquid (g cm^{-3})

t = desolvation time (sec)

A_o = initial area of droplet (cm^2)

C_p = specific heat of the vapor (cal g^{-1} $^oC^{-1}$)

λ = thermal conductivity of the gas (cal sec^{-1} cm^{-1} °C)

T = desolvation temperature (°C)

T_b = boiling point of the solvent (°C)

L = specific heat of vaporization (cal g^{-1})

I_{na} = source intensity at a non-absorbing line

I_F = source intensity at the fluorescence line (erg sec^{-1} cm^{-2} sr^{-1})

S_s = scatter signal (V, A, or arbitrary units)

S'_s = corrected scatter signal (V, A, or arbitrary units)

S_F = apparent fluorescence signal (V, A, or arbitrary units)

S'_F = corrected fluorescence signal (V, A, or arbitrary units)

S_b = blank signal (V, A, or arbitrary units)

APPENDIX II

ROTAMETER CALIBRATION

The rotameters were calibrated for various gas flows at different temperatures. The gas flow rates versus the pressure and ball heights for the Ar flow rate, nebulizer; Ar flow rate, external; H_2 flow rate, external; and CH_4 flow rate, internal, are given in Figures 30, 31, 32, 33, respectively. The first three flow rates were calibrated with a wet test meter (Precision Scientific Co.), while CH_4 was calibrated with a common bubble meter used in gas chromatography.

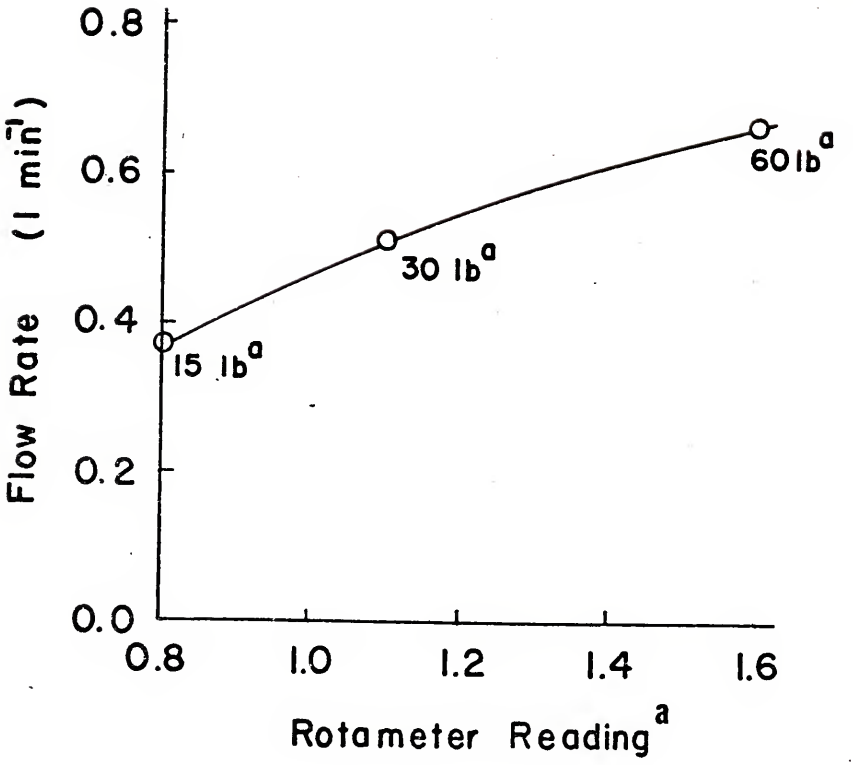

Fig. 30.--Ar nebulizer flow rate versus rotameter reading.

a - Reading = center of black ball.

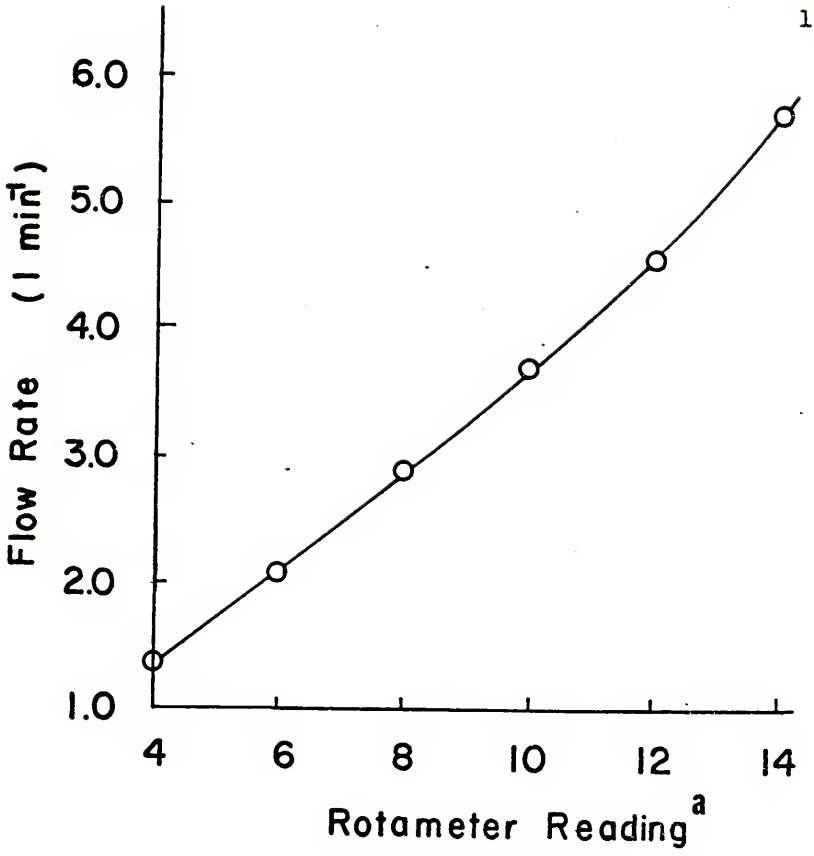

Fig. 31.--External Ar flow rate versus rotameter reading at 60 pounds.

a - Reading = center of silver ball.

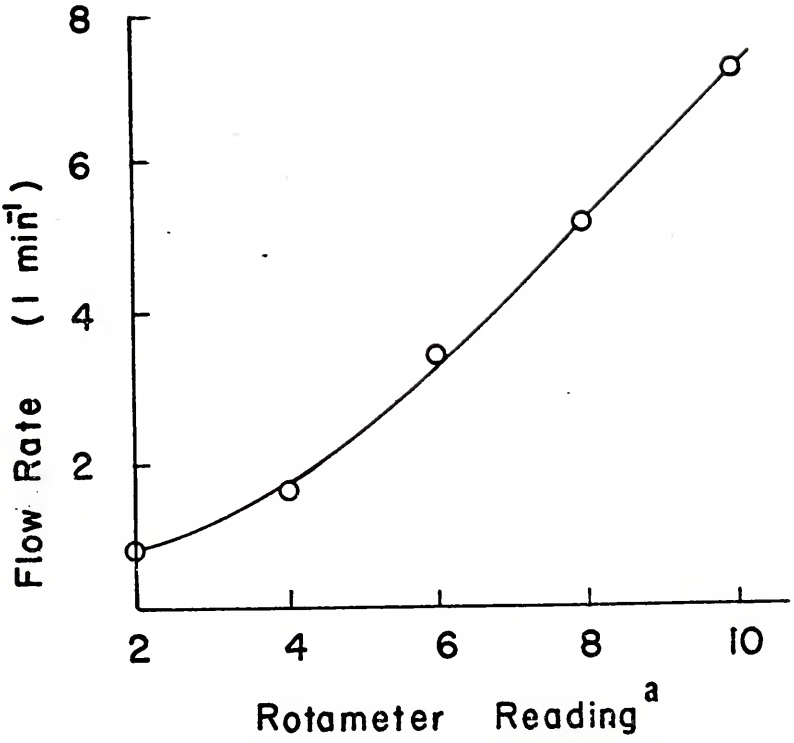

Fig. 32.--External H_2 flow rate versus rotameter reading at 12 pounds.

a - Reading = center of black ball.

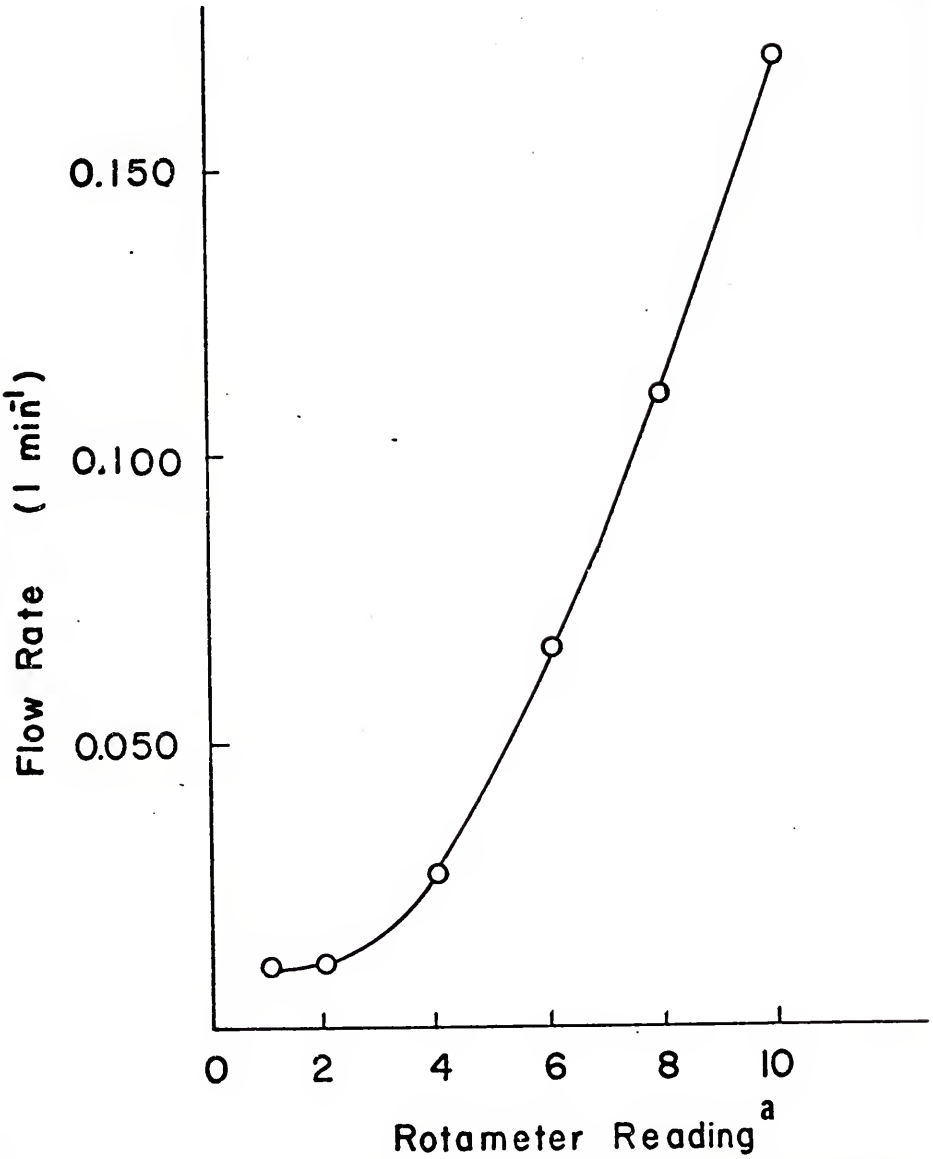

Fig. 33.--Internal CH_4 flow rate versus rotameter reading at 8 pounds.
a - Reading = center of black ball.

LITERATURE CITED

1. Hermann, R., and C. Th. J. Alkelmade, "Chemical Analysis by Flame Photometry," Interscience Publishers, New York, 1963, pp. 28, 33, 77.

2. L'vov, B. V., J. Engng. Phys., 2 (2), 441 (1959).

3. L'vov, B. V., J. Engng. Phys., 2 (11), 56 (1959).

4. L'vov, B. V., Spectrochim. Acta, 17, 761 (1961).

5. L'vov, B. V., and G. G. Lebedev, Zh. Probl. Spectroskopii, 7, 264 (1967).

6. L'vov, B. V., Spectrochim. Acta, 24B, 53 (1969).

7. L'vov, B. V., "Atomic Absorption Spectrochemical Analysis," Adam Hilger, London, 1970, 193.

8. Massmann, H., Spectrochim. Acta, 23B, 215 (1968).

9. Massmann, H., Z. Analyt. Chem., 225, 203 (1967).

10. Manning, D. C., and F. J. Fernandez, Atomic Abs. Newsl., 9, 65 (1970).

11. Seegar, D. A., and J. G. Gonzalez, Anal. Chim. Acta, 58, 7 (1972).

12. Omang, S. H., Anal. Chim. Acta, 56, 470 (1971).

13. Omang, S. H., Anal. Chim. Acta, 55, 439 (1971).

14. Kahn, H. L., and S. Slavin, Atomic Abs. Newsl., 10, 125 (1971).

15. Pickford, C. J., and G. Rossi, Analyst, 97, 647 (1972).

16. West, T. S., and X. K. Williams, Anal. Chim. Acta, 45, 27 (1969).

17. Anderson, R. G., Maines, T. S., and T. S. West, Anal. Chim. Acta, 51, 355 (1970).

18. Alder, J. F., and T. S. West, Anal. Chim. Acta, 51, 367 (1970).

19. Aggett, J., and T. S. West, Anal. Chim. Acta, 55, 349 (1971).

20. Aggett, J., and T. S. West, Anal. Chim. Acta, 57, 15 (1971).

21. Alger, D., Anderson, R. G., Maines, I. S., and T. S. West, Anal. Chim. Acta, 57, 271 (1971).

22. Anderson, R. G., Johnson, H. N., and T. S. West, Anal. Chim. Acta, 57, 281 (1971).

23. Ebdon, L., Kirkbright, G. F., and T. S. West, Anal. Chim. Acta, 58, 39 (1972).

24. Jackson, K. W., and T. S. West, Anal. Chim. Acta, 59, 187 (1972).

25. Ebdon, L., Kirkbright, G. F., and T. S. West, Anal. Chim. Acta, 61, 15 (1972).

26. Everett, G., West, T. S., and R. W. Williams, Anal. Chim. Acta, in press (1973).

27. Dagnall, R. M., Johnson, D. J., and T. S. West, Anal. Chim. Acta, in press (1973).

28. Osborne, A. C., Proc. Soc. Anal. Chem., 9, 171 (1972).

29. Jackson, K. W., West, T. S., and L. Balchin, Anal. Chem., 45, 249 (1973).

30. Molnar, C. J., Reeves, R. D., Winefordner, J. D., Glenn, M. T., Ahlstrom, J. R., and J. Savory, Appl. Spectrosc., 26, 607 (1972).

31. Reeves, R. D., Molnar, C. J., Glenn, M. T., Ahlstrom, J. R., and J. D. Winefordner, Anal. Chem., 44, 2205 (1972).

32. Patel, B.M., Reeves, R.D., Browner, R.F., Molnar, C.J., and J.D. Winefordner, Appl. Spectrosc., 27, 171 (1973).

33. Reeves, R.D., Molnar, C.J., And J.D. Winefordner, Anal. Chem., 44, 1913 (1972).

34. Reeves, R.D., Molnar, C.J., and J.D. Winefordner, Anal. Chem., 44, 1914 (1972).

35. Amos, M.D., Amer. Lab. , 33 (August, 1970).

36. Amos, M.D., Bennett, P.A., Brodie, K.G., Lung, P.W.Y., and J.P. Matousek, Anal. Chem., 43, 211 (1971).

37. Bratzel, M.P., and C.L. Chakrabarti, Anal. Chim. Acta, 61, 25 (1972).

38. Brodie, K.G., and J.P. Matousek, Anal. Chem., 43, 1557 (1971).

39. Bratzel, M.P., Chakrabarti, C.L., Sturgeon, R.E., McIntyre, M.W., and H. Agemair, Anal. Chem., 44, 372 (1972).

40. Brandenburger, H., and H. Bader, Helv. Chim. Acta., 50, 1409 (1967).

41. Bratzel, M.P., Dagnall, R.M., and J.D. Winefordner, Atomic Abs. Newsl., 7, 53 (1968).

42. Hwang, J.Y., Mokeler, C.J., and P.A. Ullucci, Anal. Chem., 44, 2018 (1972).

43. Hwang, J.Y., Ullucci, P.A., Smith, S.D., and A.L. Malenfant, Anal. Chem., 43, 1319 (1971).

44. Woodriff, R., and R.W. Stone, Appl. Opt., 7, 1337 (1968).

45. Woodriff, R., and R.W. Stone, Appl. Opt., 7, 1337 (1968).

46. Woodriff, R., and G. Ramelov, Spectrochim. Acta, 23B, 665 (1968).

47. Woodriff, R., Culver, B.R., Shrader, D., and A.B. Super, Anal. Chem., 45, 230 (1973).

48. Woodriff, R., and J.F. Lech, Anal. Chem., 43, 1918 (1971).

49. Woodriff, R., Newman, D. R., and G. Pogenkopf, Anal. Chem., 44, 2248 (1972).

50. Black, M. S., Glenn, T. H., Bratzel, M. P., and J. D. Winefordner, Anal. Chem., 43, 1769 (1971).

51. Murphy, M. K., Clyburn, S. A., and C. Veillon, Anal. Chem., 45, 1468 (1973).

52. Veillon, C., and M. Margoshes, Spectrochim. Acta, 23B, 553 (1968).

53. Winefordner, J. D., in "Atomic Absorption Spectroscopy," Plenary Lectures presented at the International Atomic Absorption Spectroscopy Conference, Sheffield, 1969, R. M. Dagnall and G. F. Kirkbright, Eds., Butterworth, London, 1970, p. 37.

54. Kirkbright, G. F., Analyst, 96, 609 (1971).

55. Winefordner, J. D., and T. J. Vickers, Anal. Chem., 44, 150R (1972).

56. Omenetto, N., and J. D. Winefordner, Appl. Spectrosc., 26, 55 (1972).

57. Winefordner, J. D., Svoboda, V., and L. J. Cline, C R C Crit. Rev., Anal. Chem., 1, 223 (1970).

58. Winefordner, J. D., and R. C. Elser, Anal. Chem., 43, 24A (1971).

59. Winefordner, J. D., and T. J. Vickers, Anal. Chem., 36, 161 (1964).

60. Zeegers, P. J. T., Smith, R., and J. D. Winefordner, Anal. Chem., 40, 26A (1968).

61. Svoboda, V., Browner, R. F., and J. D. Winefordner, Appl. Spectrosc., 26, 505 (1972).

62. Jenkins, D. R., Proc. Roy. Soc. A, 293, 493 (1966).

63. Jenkins, D. R., Spectrochim. Acta, 23B, 167 (1968).

64. McCarthy, W. J., Parsons, M. L., and J. D. Winefordner, Spectrochim. Acta, 23B, 25 (1967).

65. L'vov, B. V., P A C, 23, 11 (1970).

66. Benedict, R. R., "Electronics for Scientists and Engineers," Prentice-Hall, Inc., Englewood Cliffs, N. J., 1967, p. 22.

67. Williams, H. P., and J. D. Winefordner, J. Gas Chrom., 4, 271 (1966).

68. de Galan, L., "Analytical Spectrometry," Adam Hilger, Ltd., London, 1971, p. 123.

69. Kaiser, H., Spectrochim. Acta, 3, 40 (1947).

70. Kaiser, H., Optik, 21, 309 (1964).

71. Kaiser, H., Z. Anal. Chem., 209, 1 (1965).

72. Beckwith, P. M., Browner, R. F., and J. D. Winefordner, "High Frequency Excited Electrodeless Sources in Analytical Chemistry," Marcel Dekker, Inc., New York. (To be published.)

73. O'Haver, T. C., unpublished data, University of Maryland, College Park, Md., 1972.

74. Patel, B. M., Browner, R. F., and J. D. Winefordner, Anal. Chem., 44, 2272 (1972).

75. Browner, R. F., Patel, B. M., Glenn, T. J., Rietta, M. E., and J. D. Winefordner, Spectros. Lett., 5, 311 (1972).

76. Stupar, J., and J. B. Dawson, Appl. Opt., 7, 1351 (1968).

77. Kirsten, W. J., and G. O. B. Bertilsson, Anal. Chem., 38, 649 (1966).

78. Denton, M. B., and H. V. Malmstadt, Anal. Chem., 44, 241 (1972).

79. Dean, J. A., and T. C. Rains, "Flame Emission and Atomic Absorption Spectroscopy," Vol. II, Marcel Dekker, Inc., New York, 1971, p. 60.

80. Dean, J. A., and T. C. Rains, "Flame Emission and Atomic Absorption Spectroscopy," Vol. I, Marcel Dekker, Inc., New York, 1971, p. 106.

81. Omenetto, N., Hart, L. P., and J. D. Winefordner, Appl. Spectrosc., 26, 612 (1972).

82. Bennetti, P., Omenetto, N., and G. Rossi, Appl. Spectrosc., 25, 57 (1971).

83. Browner, R. F., Dagnall, R. M., and T. S. West, Anal. Chim. Acta, 46, 207 (1969).

84. Browner, R. F., Dagnall, R. M., and T. S. West, Anal. Chim. Acta, 50, 375 (1970).

85. Hell, A., and S. Ricchio, paper 23 given at the Pittsburgh Conference on Analytical Chemistry and Applied Spectroscopy, Cleveland, Ohio, 1970.

86. Zacha, K. H., Bratzel, M. P., Mansfield, J. M., and J. D. Winefordner, Anal. Chem., 40, 1733 (1968).

87. Bratzel, M. P., and J. D. Winefordner, Anal. Lett., 1, 43 (1967).

88. Dagnall, R. M., Thompson, K. C., and T. S. West, Talanta, 14, 1151 (1967).

89. Larkins, P. L., Spectrochim. Acta, 26B, 477 (1971).

90. Fleet, B., Liberty, K. V., and T. S. West, Anal. Chim. Acta, 45, 205 (1969).

91. Perkin Elmer Literature on AA403, Perkin Elmer Corp., Norwalk, Conn.

92. Fassel, V. A., Electrical "Flame" Spectroscopy Plenary Lectures, XVI Colloquium Spectroscopicum Internationale, Heidelberg, 1971.

93. Bowmans, P. W. J. M., and F. J. De Boer, Spectrochim. Acta, 27B, 391 (1972).

94. Mavrodineau, R., "Analaytical Flame Spectroscopy," Macmillan and Co., Ltd., London, 1970, pp. 44, 66, and 278.

95. Gilbert, P. T. Jr., "Proceedings of the Xth Colloquium Spectroscopicum Internationale," Spartan Press, Washington, D. C., 1963, p. 171.

96. Mavrodineau, R., and H. Boiteux, "Flame Spectroscopy," John Wiley and Sons, Inc., New York, 1965, pp. 15, 26, 164, 509, 545, 547, and 549.

97. O'Haver, T., and J. D. Winefordner, J. Chem. Ed., 46, 241 (1969).

BIOGRAPHICAL SKETCH

Charles J. Molnar was born in Cleveland, Ohio on February 21, 1948. He attended school in Mayfield Heights, Ohio, and graduated from Mayfield High School in 1966. He received his Bachelor of Science degree in chemistry from Ohio University in June, 1970.

In the fall of 1970, he began his graduate studies at the University of Florida, and has worked toward his doctoral degree in analytical chemistry since that time.

He married Judith Ratcliffe in December, 1970.

I certify that I have read this study and that in my opinion it conforms to acceptable standards of scholarly presentation and is fully adequate, in scope and quality, as a dissertation for the degree of Doctor of Philosophy.

James D. Winefordner, Chairman
Professor of Chemistry

I certify that I have read this study and that in my opinion it conforms to acceptable standards of scholarly presentation and is fully adequate, in scope and quality, as a dissertation for the degree of Doctor of Philosophy.

Roger G. Bates
Professor of Chemistry

I certify that I have read this study and that in my opinion it conforms to acceptable standards of scholarly presentation and is fully adequate, in scope and quality, as a dissertation for the degree of Doctor of Philosophy.

Gerhard M. Schmid
Associate Professor of Chemistry

I certify that I have read this study and that in my opinion it conforms to acceptable standards of scholarly presentation and is fully adequate, in scope and quality, as a dissertation for the degree of Doctor of Philosophy.

John E. Singley
Professor of Environmental Engineering Science

I certify that I have read this study and that in my opinion it conforms to acceptable standards of scholarly presentation and is fully adequate, in scope and quality, as a dissertation for the degree of Doctor of Philosophy.

John C. Gudat
Assistant Professor of Pathology

This dissertation was submitted to the Graduate Faculty of the Department of Chemistry in the College of Arts and Sciences and to the Graduate Council, and was accepted as partial fulfillment of the requirements for the degree of Doctor of Philosophy.

June, 1974

Dean, Graduate School